SSSTJ
VOL.7 NO.2
July 2020
ISSN 2351-0889

SSSTJ

Suan Sunandha Science and Technology Journal

Volume 7, Number 2, July 2020

Suan Sunandha Science and Technology Journal

General Information

The Suan Sunandha Science and Technology Journal (SSSTJ) is a double-blind peer reviewed scientific journal published twice a year (January and July) by the Faculty of Science and Technology, Suan Sunandha Rajabhat University. Submissions of manuscripts should be sent to the Editor of the SSSTJ by online system: http://www.ssstj.sci.ssru.ac.th. The manuscript will be taken that all contributing authors attest that manuscripts and material submitted to the SSSTJ are original and have not been published or submitted elsewhere and the authors concede to the open-access distribution of the manuscript, including all contents contained therein.

Aim and scope:

Suan Sunandha Science and Technology Journal (SSSTJ) is an international academic journal that gains foothold at Suan Sunandha Rajabhat University, Thailand and opens to scientific communications in Southeast Asia, Asia and worldwide. It aims to contribute significant articles in science and technology researches. Published papers are focused on state of the art science and technology. Committee of the journal and association will review submitted papers. The authors may include researchers, managers, operators, students, teachers and developers.

Following areas are considered for publication:
1. Applied Physics
2. Applied Statistics
3. Biology
4. Biotechnology
5. Chemistry
6. Computer Science
7. Energy
8. Environmental Science and Technology
9. Information Technology
10. Mathematics
11. Microbiology
12. Food Science and Technology
13. Forensic Science
14. Sport Science
15. Other related fields

QR CODE Journal

Suan Sunandha Science and Technology Journal

Editorial Board

SUAN SUNANDHA SCIENCE AND TECHNOLOGY JOURNAL
Suan Sunandha Rajabhat University, Faculty of Science and Technology
1 U-thong Nok Road, Dusit, Bangkok 10300 THAILAND

CONTENTS

Volume 7, No.2 **July 2020**

Available online at http://www.ssstj.sci.ssru.ac.th

SSSTJ

Suan Sunandha Science and Technology Journal

Two New Iterative Methods for Solving Nonlinear Equations without Derivative

Jirawat Kantalo[1], Sa-at Muangchan[1], Supunnee Sompong [1]

[1]Faculty of Science and Technology, Sakon Nakhon Rajabhat University

[1]Nittayo Road, Sakon Nakhon, 47000, Thailand

Corresponding author e-mail: *jirawatkantalo@gmail.com

Received: *6 January 2020* / **Revised:** *1 March 2020* / **Accepted:** *4 April 2020*

Abstract

In this paper, we propose two new iterative methods for solving nonlinear equations with one variable without derivative. In convergence theory, the two new iterative methods have second and third order convergence. Some numerical experiments show that the two new derivative free iterative methods outperform the several other existing methods.

Keywords: Non-linear Equations, Order of Convergence, Derivative Free Method

1. Introduction

Solving a nonlinear equation $f(x)=0$ is the most important problems in Numerical analysis. Since it is not always possible to find the exactly solution by the direct method, the numerical iterative methods are useful to obtain an approximate solution of equations. There are many different iterative methods for solving nonlinear equations. One of the classical standard numerical iterative methods is a Newton's method, it given by

$$x_{n+1} = x_n - \frac{f(x_n)}{f'(x_n)}, \quad n \in \mathbb{N} \tag{1}$$

where x_0 is an initial value that we might guess the initial value which near a solution of equations. This method has second order of convergence (Argyros, 2008). However, the Newton's method has a disadvantage, one has to calculate the derivative of $f(x)$. Sometimes, the first derivative function of $f(x)$ is more difficult to calculate or $f(x)$ is not differentiable at a certain point, the Newton's method is not applicable to solve nonlinear equation. Therefore, the Newton's method was modified by many researchers who considered the first derivative function by approximation of derivatives. (Jain, 2007; Hafiz, 2014; Singh, 2017)

Steffensen's method is one of the iterative methods which is based on the Newton's method (Conte & Boor, 1981). The method was modified by substitute the derivative function of function in the Newton's method by using a forward difference approximation, it given by

$$f'(x_n) \approx \frac{f(x_n + f(x_n)) - f(x_n)}{f(x_n)}. \tag{2}$$

Therefore, the Steffensen's method becomes

$$x_{n+1} = x_n - \frac{f(x_n)^2}{f(x_n + f(x_n)) - f(x_n)}, \quad n \in \mathbb{N}. \tag{3}$$

The method still has second order convergence. In 2005, the new iterative method formed by the composition of the Newton's method and the Steffensen's method, namely Newton-Steffensen's method was introduced by Sharma (Sharma, 2005). It given by

$$y_n = x_n - \frac{f(x_n)}{f'(x_n)}, \tag{4}$$

$$x_{n+1} = x_n - \frac{f(x_n)^2}{f'(x_n)(f(x_n) - f(y_n))}, \quad n \in \mathbb{N} \tag{5}$$

which has third order of convergence.

In 2010, Dehghan and Hajarian (Dehghan & Hajarian, 2010) introduced two new third order of convergence methods, called Dehghan *I* 's method and Dehghan *II* 's method. The Dehghan *I* 's method is given by

$$y_n = x_n - \frac{2f(x_n)^2}{f(x_n + f(x_n)) - f(x_n - f(x_n))}, \tag{6}$$

$$x_{n+1} = x_n - \frac{2f(x_n)\left(f(x_n) + f(y_n)\right)}{f(x_n + f(x_n)) - f(x_n - f(x_n))}, \quad n \in \mathbb{N}, \tag{7}$$

and the Dehghan *II* 's method is given by

$$y_n = x_n + \frac{2f(x_n)^2}{f(x_n + f(x_n)) - f(x_n - f(x_n))}, \tag{8}$$

$$x_{n+1} = x_n - \frac{2f(x_n)\left(f(x_n) + f(y_n)\right)}{f(x_n + f(x_n)) - f(x_n - f(x_n))}, \quad n \in \mathbb{N}. \tag{9}$$

Suan Sunandha Science and Technology Journal

In this paper, we introduce two new derivative free iterative methods for solving nonlinear equations which replaced the derivative function $f'(x)$ by using the half forward difference and an average between forward and central difference approximation.

The remainder of this paper is organized as follow. In section 2, the two new derivative free iterative methods are provided and order of convergence for iterative methods are established. In section 3, numerical examples show that both methods are better performance than of each of the existing methods described. Finally, conclusion is given in section 4.

2. Description of the methods and convergence analysis

In this section, we shall describe derivative free iterative methods which by using different approximation of derivatives. Moreover, we show that convergence analysis of our methods. Letting $x^* \in I$ be a simple zero of a sufficiently differentiable function $f : I \subseteq \mathbb{R} \to \mathbb{R}$ in an open interval I.

2.1 A two order of convergence derivative free iterative method (Method I)

To construct the second order convergence derivative free iterative method, we consider the approximation of derivative in the Steffensen's method as form (3) and modify this method by using the half forward difference approximation as figure 1.

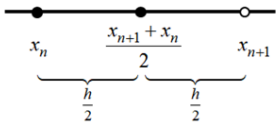

Figure 1. The half forward difference approximation.

By approximation of the derivative, we have

$$f'(x_n) \approx \frac{f\left(\frac{x_{n+1}+x_n}{2}\right) - f(x_n)}{\frac{h}{2}} \approx \frac{2\left(f\left(\frac{2x_n+h}{2}\right) - f(x_n)\right)}{h}, \tag{10}$$

where h is a very small value. As n is a large number and x_0 is close enough to the root x^* we will estimate value of h by $f(x_n)$ So, we have

$$f'(x_n) \approx \frac{2\left(f\left(\frac{2x_n+f(x_n)}{2}\right) - f(x_n)\right)}{f(x_n)}. \tag{11}$$

Then we obtain the new derivative free iterative method as form

$$x_{n+1} = x_n - \frac{f(x_n)^2}{2\left(f\left(\frac{2x_n+f(x_n)}{2}\right) - f(x_n)\right)}, \ n \in \mathbb{N}. \tag{12}$$

2.2 A three order of convergence derivative free iterative method (Method II)

To construct the third order convergence derivative free iterative method, we consider the Newton-Steffensen's method as form (4),(5) and use the average of forward and central different as figure 2 to approximate the derivative of function at the n^{th} iteration.

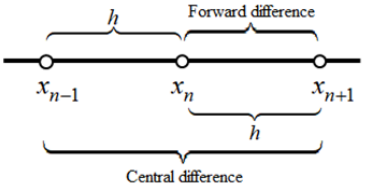

Figure 2. The forward and central difference approximation.

So, the average of forward and central difference approximation is given by

$$\begin{aligned} f'(x_n) &\approx \frac{1}{2}\left(\frac{f(x_n+h)-f(x_n)}{h} + \frac{f(x_n+h)-f(x_n-h)}{2h}\right) \\ &\approx \frac{1}{2}\left(\frac{2f(x_n+h)-2f(x_n)+f(x_n+h)-f(x_n-h)}{2h}\right) \\ &\approx \frac{1}{2}\left(\frac{3f(x_n+h)-2f(x_n)-f(x_n-h)}{2h}\right) \\ &\approx \left(\frac{3f(x_n+h)-2f(x_n)-f(x_n-h)}{4h}\right), \end{aligned} \tag{13}$$

where h is a very small value. Then we substitute the value of h by $f(x_n)$ So, we have

$$f'(x_n) \approx \frac{3f(x_n+f(x_n))-2f(x_n)-f(x_n-f(x_n))}{4f(x_n)}. \tag{14}$$

Therefore, the derivative function in Newton-Steffensen's method as form (4),(5) was replaced by the above approximating the derivative. The new derivative free iterative method becomes

$$y_n = x_n - \frac{4f(x_n)^2}{3f(x_n+f(x_n))-2f(x_n)-f(x_n-f(x_n))} \tag{15}$$

$$x_{n+1} = x_n - \frac{4f(x_n)^2}{(3f(x_n+f(x_n))-2f(x_n)-f(x_n-f(x_n)))(f(x_n)-f(y_n))}, \tag{16}$$

where $n \in \mathbb{N}$.

In the following theorems, we are going to prove that the our iterative methods have orders of convergence 2 and 3, respectively.

Suan Sunandha Science and Technology Journal

Theorem 2.1 If x_0 is sufficiently close to x^*, then the derivative free iterative method (Method I) has second order of convergence.

Proof. Let x^* be the simple root of $f(x)$, i.e. $f(x^*)=0,\ f'(x^*)\neq 0$, and the error equation is $e_n = x_n - x^*$. Using Taylor series of $f(x_n)$ about x^*, we have

$$f(x_n) = c_1 e_n + c_2 e_n^2 + c_3 e_n^3 + c_4 e_n^4 + c_5 e_n^5 + c_6 e_n^6 + O(e_n^7), \tag{17}$$

where $c_k = \frac{f^k(x^*)}{k!}$, $k = 1,2,3,\ldots$.

Computing $f(x_n)^2$, it is given as following

$$f(x_n)^2 = c_1^2 e_n^2 + 2c_1c_2 e_n^3 + (2c_1c_3 + c_2^2)e_n^4 + (2c_1c_4 + 2c_2c_3)e_n^5 + O(e_n^6). \tag{18}$$

Using equation (17) to compute $2\left(f\left(\frac{2x_n + f(x_n)}{2}\right) - f(x_n)\right)$. Then this term can be obtained after simplifying follows :

$$\begin{aligned} &2\left(f\left(\frac{2x_n + f(x_n)}{2}\right) - f(x_n)\right) \\ &= c_1^2 e_n + \left(3c_1c_2 + \frac{c_1^2c_2}{2}\right)e_n^2 + \left(4c_1c_3 + 2c_2^2 + c_1c_2^2 + \frac{3c_1^2c_3}{2} \right. \\ &\left. + \frac{c_1^3c_3}{4}\right)e_n^3 + \left(5c_1c_4 + 5c_2c_3 + 4c_1c_2c_3 + \frac{c_2^3}{2} + \frac{3c_1^2c_2c_3}{4} + 3c_1^2c_4 \right. \\ &\left. + c_1^3c_4 + \frac{c_1^4c_4}{8}\right)e_n^4 + O(e_n^5). \end{aligned} \tag{19}$$

Substituting (18) and (19) in the equation (12), we have

$$e_{n+1} = \left(\frac{c_2}{c_1} + \frac{c_2}{2}\right)e_n^2 + O(e_n^{2+1}). \tag{20}$$

Hence, it follows that the derivative free iterative method which is of the form (12) has second order of convergence.

Theorem 2.2 If x_0 is sufficiently close to x^*, then the derivative free iterative method (Method II) has third order of convergence.

Proof. Let x^* be the simple root of $f(x)$, i.e. $f(x^*)=0,\ f'(x^*)\neq 0$, and the error equation is $e_n = x_n - x^*$. Using Taylor series of $f(x_n)$ about x^*, we have

$$f(x_n) = c_1 e_n + c_2 e_n^2 + c_3 e_n^3 + c_4 e_n^4 + c_5 e_n^5 + c_6 e_n^6 + O(e_n^7), \tag{21}$$

where $c_k = \frac{f^k(x^*)}{k!}$, $k = 1,2,3,\ldots$.

Computing $f(x_n)^2$, it is given as following

$$f(x_n)^2 = c_1^2 e_n^2 + 2c_1c_2 e_n^3 + (2c_1c_3 + c_2^2)e_n^4 + (2c_1c_4 + 2c_2c_3)e_n^5 + O(e_n^6). \tag{22}$$

Computing $f(x_n + f(x_n))$ and $f(x_n - f(x_n))$, can be obtained after simplifying as following

$$\begin{aligned} &f(x_n + f(x_n)) \\ &= (c_1^2 + c_1)e_n + (c_2c_1^2 + 3c_2c_1 + c_2)e_n^2 + (c_3c_1^3 + 3c_3c_1^2 \\ &+ 2c_1c_2^2 + 4c_3c_1 + 2c_2^2 + c_3)e_n^3 + (c_4 + c_2(c_2^2 + 2c_1c_3) \\ &+ 5c_1c_4 + 5c_2c_3 + 6c_1^2c_4 + 4c_1^3c_4 + c_1^4c_4 + 6c_1c_2c_3 \\ &+ 3c_1^2c_2c_3)e_n^4 + O(e_n^5) \end{aligned} \tag{23}$$

and

$$\begin{aligned} &f(x_n - f(x_n)) \\ &= (-c_1^2 + c_1)e_n + (c_2c_1^2 - 3c_2c_1 + c_2)e_n^2 + (-c_3c_1^3 + 3c_3c_1^2 \\ &+ 2c_1c_2^2 - 4c_3c_1 - 2c_2^2 + c_3)e_n^3 + (c_4 + c_2(c_2^2 + 2c_1c_3) \\ &- 5c_1c_4 - 5c_2c_3 + 6c_1^2c_4 - 4c_1^3c_4 + c_1^4c_4 + 6c_1c_2c_3 \\ &- 3c_1^2c_2c_3)e_n^4 + O(e_n^5). \end{aligned} \tag{24}$$

Using equation (21),(22),(23) and (24) to compute

$\frac{4f(x_n)^2}{3f(x_n + f(x_n)) - 2f(x_n) - f(x_n - f(x_n))}$. Then we have

$$\begin{aligned} &\frac{4f(x_n)^2}{3f(x_n + f(x_n)) - 2f(x_n) - f(x_n - f(x_n))} \\ &= e_n + \left(-\frac{c_2}{c_1} - \frac{c_2}{2}\right)e_n^2 + \left(-\frac{2c_3}{c_1} + \frac{2c_2^2}{c_1^2} + \frac{c_2^2}{c_1} + \frac{3c_3}{2} \right. \\ &\left. - c_1c_3 + \frac{c_2^2}{4}\right)e_n^3 + \left(-\frac{3c_4}{c_1} + \frac{7c_2c_3}{c_1^2} + \frac{5c_2c_3}{c_1} - \frac{11c_2^3}{2c_1^2} \right. \\ &\left. + \frac{5c_2c_3}{2} - 3c_4 - 4c_1c_4 - \frac{c_1^2c_4}{2} - \frac{4c_2^3}{c_1^3} - \frac{3c_2^3}{4c_1} + \frac{6c_3}{c_1} \right. \\ &\left. - \frac{c_2^3}{8}\right)e_n^4 + O(e_n^5) \end{aligned} \tag{25}$$

By considering y_n in the equation (15), we have

Suan Sunandha Science and Technology Journal

$$y_n = x^* + \left(\frac{c_2}{c_1}+\frac{c_2}{2}\right)e_n^2 + \left(\frac{2c_3}{c_1}-\frac{2c_2^2}{c_1^2}-\frac{c_2^2}{c_1}-\frac{3c_3}{2}+c_1c_3 - \frac{c_2^2}{4}\right)e_n^3 + \left(\frac{3c_4}{c_1}-\frac{7c_2c_3}{c_1^2}-\frac{5c_2c_3}{c_1}+\frac{11c_2^3}{2c_1^2}-\frac{5c_2c_3}{2} + 3c_4+4c_1c_4+\frac{c_1^2c_4}{2}+\frac{4c_2^3}{c_1^3}+\frac{3c_2^3}{4c_1}-\frac{6c_3}{c_1}+\frac{c_2^3}{8}\right)e_n^4 + O(e_n^5). \quad (26)$$

Now, substituting (26) in Taylor series of $f(y_n)$, we have

$$f(y_n) = \left(c_2+\frac{c_1c_2}{2}\right)e_n^2 + \left(2c_3-\frac{2c_2^2}{c_1}-c_2^2-\frac{3c_1c_3}{2}+c_1^2c_3 - \frac{c_1c_2^2}{4}\right)e_n^3 + \left(3c_4-\frac{7c_2c_3}{c_1}-5c_2c_3+\frac{11c_2^3}{2c_1}+\frac{5c_1c_2c_3}{2} + 3c_1c_4+4c_1^2c_4+\frac{c_1^3c_4}{2}+\frac{5c_2^3}{c_1^2}+c_2^3-6c_3+\frac{c_1c_2^3}{8}+\frac{c_2^3}{c_1}\right)e_n^4 + O(e_n^5). \quad (27)$$

Using equation (25) and (27) in the equation (16), we have

$$e_{n+1} = \left(\frac{c_2^2}{c_1^2}+\frac{c_2^2}{2c_1}+3c_3\right)e_n^3 + O(e_n^{3+1}). \quad (28)$$

Hence, it follows that the derivative free iterative method which is form of (15), (16) has the third order convergence.

3. Numerical examples

To numerical comparison, we will present some problems of nonlinear equations from the tested function of Jaiswal (Jaiswal, 2013) and Dehghan and Hajarian (Dehghan & Hajarian, 2010) to compare the proposed methods with existing methods which are as follows: the Newton's method is of the form (2), the Steffensen's method is of the form (3), the Newton-Steffensen's method is of the form (4),(5) and the two Dehghan's methods, namely the Dehghan *I* 's method and the Dehghan *II* 's method which are of the form (6),(7) and (8),(9), respectively. In these comparisons, we consider the following functions

Table 1. Test functions and their roots.

Functions	Root
$f_1(x) = \sin^2(x) - x^2 + 1$	1.404492
$f_2(x) = \cos(x) - x$	0.739085
$f_3(x) = \cos(x) - xe^x + x^2$	0.639154
$f_4(x) = e^x - 1.5 - \arctan(x)$	0.767653
$f_5(x) = \ln(x^2 + x + 2) - x + 1$	4.152590
$f_6(x) = x^2 - e^x - 3x + 2$	0.257530

In order to compare of the numerical iterative methods, the numerical experiments have been implemented on GNU Octave, version 5.1.0 with different initial value x_0. Then we choose initial value x_0 that will be a suitable test for these functions. We consider the number of iterations n and the absolute value of function $|f(x_n)|$ when $|f(x_n)| \le 10^{-12}$. The algorithm for the our iterative methods are as follows:

Numerical Algorithm of Method I

Input: The nonlinear function $f(x)$, tolerance TOL and initial value of x_0.

Step 1 Set $n = 0$.

Step 2 While $|f(x_0)| > TOL$ do Step 3-4.

Step 3 Calculate

$$x_{n+1} = x_n - \frac{f(x_n)^2}{2\left(f\left(\frac{2x_n + f(x_n)}{2}\right) - f(x_n)\right)}.$$

Calculate $|f(x_{n+1})|$.

Set $n = n+1$.

Step 4 If $|f(x_{n+1})| \le TOL$, then we stop the iteration and print the output of the root of function x_{n+1}, the absolute value of function $|f(x_{n+1})|$ and the number of iterations n.

Numerical Algorithm of Method II

Input: The nonlinear function $f(x)$, tolerance TOL and initial value of x_0.

Step 1 Set $n = 0$.

Step 2 While $|f(x_0)| > TOL$ do Step 3-4.

Step 3 Calculate

$$y_n = x_n - \frac{4f(x_n)^2}{3f(x_n + f(x_n)) - 2f(x_n) - f(x_n - f(x_n))}$$

and

$$x_{n+1} = x_n - \frac{4f(x_n)^2}{(3f(x_n + f(x_n)) - 2f(x_n) - f(x_n - f(x_n)))(f(x_n) - f(y_n))},$$

Calculate $|f(x_{n+1})|$.

Set $n = n+1$.

Suan Sunandha Science and Technology Journal

Step 4 If $|f(x_{n+1})| \le TOL$, then we stop the iteration and print the output of the root of function x_{n+1}, the absolute value of function $|f(x_{n+1})|$ and the number of iterations n.

In general, the method with minimum for the number of iteration could be chosen as the best method to find solution of function. Moreover, the method gives the absolute value of function which is closer to zero than the other, is will be the best method.

Table 2. Numerical results of $f_1(x) = \sin^2(x) - x^2 + 1$ with $x_0 = 1$.

Methods	Number of iterations n	$\|f(x_n)\|$
Newton's method	5	7.593925×10^{-13}
Steffensen's method	5	9.992007×10^{-16}
Newton-Steffensen's method	5	1.323386×10^{-13}
Dehghan *I* 's method	4	4.440892×10^{-16}
Dehghan *II* 's method	4	6.302736×10^{-13}
Method *I*	4	3.330669×10^{-16}
Method *II*	3	3.330669×10^{-16}

Table 3. Numerical results of $f_2(x) = \cos(x) - x$ with $x_0 = 0$.

Methods	Number of iterations n	$\|f(x_n)\|$
Newton's method	5	0
Steffensen's method	4	1.110223×10^{-16}
Newton-Steffensen's method	5	0
Dehghan *I* 's method	4	0
Dehghan *II* 's method	3	2.109424×10^{-15}
Method *I*	4	1.110223×10^{-16}
Method *II*	3	0

Table 4. Numerical results of $f_3(x) = \cos(x) - xe^x + x^2$ with $x_0 = -2$.

Methods	Number of iterations n	$\|f(x_n)\|$
Newton's method	7	1.110223×10^{-16}
Steffensen's method	7	1.110223×10^{-16}
Newton-Steffensen's method	7	1.110223×10^{-16}
Dehghan *I* 's method	5	1.110223×10^{-16}
Dehghan *II* 's method	8	1.110223×10^{-16}
Method *I*	4	1.110223×10^{-16}
Method *II*	4	1.221245×10^{-15}

Table 5. Numerical results of $f_4(x) = e^x - 1.5 - \arctan(x)$ with $x_0 = 1$.

Methods	Number of iterations n	$\|f(x_n)\|$
Newton's method	12	1.465494×10^{-13}
Steffensen's method	6	2.220446×10^{-16}
Newton-Steffensen's method	4	2.220446×10^{-16}
Dehghan *I* 's method	3	1.110223×10^{-16}
Dehghan *II* 's method	3	5.073719×10^{-14}
Method *I*	5	4.440892×10^{-16}
Method *II*	3	0

Table 6. Numerical results of $f_5(x) = \ln(x^2 + x + 2) - x + 1$ with $x_0 = 0$.

Methods	Number of iterations n	$\|f(x_n)\|$
Newton's method	5	4.440892×10^{-16}
Steffensen's method	5	4.440892×10^{-16}
Newton-Steffensen's method	5	0
Dehghan *I* 's method	4	4.440892×10^{-16}
Dehghan *II* 's method	4	4.440892×10^{-16}
Method *I*	5	0
Method *II*	3	8.171241×10^{-14}

Table 7. Numerical results of $f_6(x) = x^2 - e^x - 3x + 2$ with $x_0 = 2$.

Methods	Number of iterations n	$\|f(x_n)\|$
Newton's method	4	3.728129×10^{-13}
Steffensen's method	6	0
Newton-Steffensen's method	14	0
Dehghan *I* 's method	17	0
Dehghan *II* 's method	1330	0
Method *I*	4	2.392082×10^{-14}
Method *II*	4	0

From Table 2-7 of numerical results, we can see that the Method *II* is better than the other iterative methods. However, the Method *I* is as good as the

Suan Sunandha Science and Technology Journal

Method *II* for $f_3(x) = \cos(x) - xe^x + x^2$ with initial $x_0 = -2$ and $f_6(x) = x^2 - e^x - 3x + 2$ with initial $x_0 = 2$. So for the different nonlinear functions, the proposed iterative method (Method *II*) outperform the other iterative methods.

4. Conclusion

In this paper, the new numerical iterative methods for solving nonlinear equations with one variable without derivative, namely Method *I* and Method *II* are presented. Moreover, the convergence analysis of our methods have been established to show that the Method *I* and Method *II* have second and third order convergence, respectively. The six nonlinear functions are considered to illustrate that Method *II* is better than some other methods. But the Method *II* is more complicated than the Method *I*. However the result from Method *I* gave as efficiency as the Method *II* . For the future work, one may consider to modify the approximating of derivative of function or extended the method to find all solutions of nonlinear equations which contain one or more than one variables.

5. References

Argyros, I.K. (2008). *Convergence and Application of Newton-Type Iteration.* Newyork: Springer.

Conte, S.D., & Boor Carl de. (1981). An Algorithmic Approach. *Elementary Numerical Analysis*. McGraw-Hill.

Dehghan, M., & Hajarian, M. (2010). Some derivative free quadratic and cubic convergence iterative formulars for solving nonlinear equations. *Computational and Applied Mathematics*, 29, 19-30.

Hafiz, M.A. (2014). Solving Nonlinear Equations Using Steffensen-Type Methods With Optimal Order of Convergence. *Palestine Journal of Mathematics, 3*(1), 113-119.

Jain, P. (2007). Steffensen type methods for solving non-linear equations. *Appl. Math. Comput*., 194, 527-533.

Jaiswal, J.P. (2013). A New Third-Order Derivative Free method for Solving Nonlinear Equations. *Universal Journal of Applied Mathematics*, *1*(2), 131-135.

Qian, Y.H., & Guo, Q.W. (2016). A new derivative-free iterative method for solving nonlinear equations. *Nonlinear Sci.Lett. A*, *7* (2), 32-40.

Sharma, J.R. (2005). A composite third order Newton Steffensen method for solving nonlinear equations. *Appl. Math. Comput*., *169* (1), 242-246.

Singh, B. (2017). Fourth-order Steffensen type methods for nonlinear equations. *International Journal of Statistics and Applied Mathematics*, *2*(4), 11-15.

Available online at http://www.ssstj.sci.ssru.ac.th

SSSTJ

Suan Sunandha Science and Technology Journal

The Preparation of Hybrid Material of Cobalt Complex into Mesoporous Silica from the Rice Husk

Pornpan Tana[1], Netchanok Jansawang[1], and Patcharaporn Pimchan[1,*]

[1]Department of chemistry, faculty of Science and Technology, Rajabhat Maha Sarakham University, Maha Sarakham 44000, Thailand

Corresponding author e-mail: *patcharaporn145@gmail.com

Received: *8 November 2019* / **Revised:** *2 February 2020* / **Accepted:** *7 April 2020*

Abstract

A luminescence hybrid material, Bis(8-hydroxyquinoline)cobalt(II) ($Co(8hq)_2$), was incorporated into the mesoporous silica. To study the preparation of mesoporous silica from rice husk and the development of fluorescence efficiency. The mesoporous silica was prepared by swelling-shrinking mechanism which used the sodium silicate from rice husk as the precursor. The hybrid materials were prepared by solid-state reaction at room temperature with two different routes; the first one was the hybrid material processes via the in situ formation of cobalt(II)chloride hexahydrate ($CoCl_2 \cdot 6H_2O$) as well as 8hq into the mesoporous silica (MCM) mixed ground ($MCM\_Co(8hq)_2$) and the another one was step by step ground of the mesoporous silica, cobalt(II)chloride hexahydrate and 8hq (MCMCo(II)_8hq). The hybrid materials were characterized by SEM, XRD, FT-IR, AAS, as well as PL. The FT-IR spectra showed the 8hq characteristic at 820, 786, 784, and 747 cm^{-1} that all of the FT-IR spectra shifted to higher frequencies of free 8hq (815, 778, and 739 cm^{-1}), confirming the coordination between cobalt(II) cation and 8-hydroxyquinoline. The excellent photoluminescence of $MCM\_Co(8hq)_2$ revealed at 484 nm and MCMCo(II)_8hq demonstrated blue-shifted peak at 474 nm in this comparison, indicating that the formation of different nanostructures and/or packing of bis (8-hydroxyquinoline)cobalt(II) were formed into the mesoporous silica.

Keywords: Hybrid material, Mesoporous silica, Bis(8-hydroxyquinoline)cobalt(II), Rice husk

1. Introduction

In recent years, the luminescence of metal complexes has attracted significant attention due to the coordination chemistry of inorganic and organic components, electron-transfer substitution of metal or ligand provides an effective means can serve as an efficient approach for the development of electroluminescent materials (Singh et al., 2018; Li & Li, 2009). As a common ligand in metal complexes are widely used aromatic rings such as 8-hydroxyquinoline (8hq), pyridine, and benzoic acid that have conjugate double-bonds as well as stronger absorption than metal ions in the ultraviolet (UV) region (Li & Li, 2009; Świderski et al., 2018; He et al., 2018). Among these ligands, 8hq has attracted much attention because of a variety of one-dimensional (1D) nanostructures of the metal-8-hydroxyquinoline complexes have been obtained such as nanorods, nanowire, and nanoribbon that nanostructures of the complexes are also tunable electronic and optical properties (Li et al., 2012; Tsuboi et al., 2012; Behzad et al., 2014; Pimchan et al., 2014).

The metal complexes illustrate potential applications in organic light-emitting devices (OLED) and efficient light-conversion molecular devices. However, their practical application in many fields limited by the low light and thermal stability and poor mechanical strength of metal complexes (He et al., 2018; Pimchan et al., 2014). A wide variety of metal chelates were prepared base-on the nanospace of mesoporous silica, boron nitrite porous, and inter layer as an appropriate host solid that an effective way to solve and protect the metal complexes (He et al., 2018; Pimchan et al., 2014; Sábio et al., 2016). These hybrid materials also have been reported to have many possible applications as photocatalyst and so on (Patriarca et al., 2019; Maučec et al., 2018).

As an emerging host, mesoporous silica has attracted much research because of the possibility of tailoring the pore structure, framework composition, and morphologies over a wide range (Lui et al.,

Suan Sunandha Science and Technology Journal

2015; Sohmiya et al., 2015; Kazuyuki et al., 2011). The porous surface of mesoporous silica could be modified by a swelling-shrinking mechanism with proper organic functional groups and provide accessibility for anchoring other substances. This technique offers the advantages of high control of the hybrid chemical composition at low temperature and large-area processing (Sohmiya et al., 2015; Kazuyuki et al., 2011). Accordingly, host-guest complexes have been synthesized from mesoporous silica for such purposes as sensors, adsorption, and optical applications (Zhao et al., 2017; Kudo et al., 2017; Li et al., 2017). Moreover, the immobilization of luminary on rigid support is a very important way to prepare new solid luminescent materials (Li et al., 2017; Zhang et al., 2018). Recently, the preparation of metal complexes base-on mesoporous silica to improve their performances have attracted increased attention. For example, the aluminum quinolate complex was attached covalently to this functionalized SBA-15 by using coordinating ability of bifunctional precursor (Si-SQ) on the surface of mesoporous material and the observed blue-shift in the emission spectra of the prepared $Al(8hq)_3$ functionalized material is attributed to the improved molecular interactions of grafted $Al(8hq)_3$ complexes on the surface and electron withdrawing effect of sulfonamide group that covalently linked to the 8hq in grafted precursor (Si-SQ) (Badiei et al. 2011). The adsorption of $[Ru(bpy)_3]^{2+}$ onto aluminum containing mesoporous silicas was conducted and the photoluminescence of the products was examined as a function of the loaded $[Ru(bpy)_3]^{2+}$ amounts. The result suggests that the pore size and the interactions between $[Ru(bpy)_3]^{2+}$ and the pore surface affects the efficiency; the larger pore size and the weaker interactions between and the pore surface results in the higher self-quenching efficiency (Sohmiya and Ogawa, 2011). Thus, the luminescence properties and stabilities of mesoporous silica-based hybrids can be meticulously designed and tuned.

Solid-state reaction is a facile and feasible method for preparing nanomaterial and has achieved some success in fabricating complex materials (Rahman, 2016). It showed that the promising luminescent properties can be obtained by linking the metal complexes to the mesoporous materials (Ma et al., 2019; Vibulyaseak et al., 2019). Therefore, the synthesis of metal complexes in mesoporous silica via solid-state may be predominant features such as high color quality, wide-viewing angle, wide operating temperature range, and fast response.

In this paper, we reported the preparation of the cobalt (II) complex of 8-hydroxyquinoline (8hq) into mesoporous silica with different methods. The mesoporous silica was prepared from rice husk which was calcined in air. The cobalt (II) complexes of 8-hydroxyquinoline in mesoporous silica were prepared by solid-state between mesoporous silica and Co (II):8hq. The different methods may enhance the luminescence efficiency of $Co(8hq)_2$ complex by reducing the concentration quenching and self-absorption. The role of preparation processes may affect the molecular structures and/or packing, as well as optical properties of $Co(8hq)_2$ complex into the porous space.

Table 1. Color and Photoluminescence band of hybrid materials.

Substances	color	λ_{em} (nm)
$Co(8hq)_2$	Dark green	492
MCM_$Co(8hq)_2$	Orange green	484
MCMCo(II)_8hq	Light green	474

2. Methodology (Materials and Methods)

2.1 Materials

Rice husk (RH) used in this research were obtained from the rice milling process in Thailand. Cetyltrimethylammonium bromide ($C_{19}H_{42}NBr$, CTAB) was supplied from Sigma-Aldrich Co., Ltd. Cobalt(II)chloride hexahydrate ($CoCl_2{\cdot}6H_2O$) was obtained from CARLO ERBA Reagents S.r.l. 8-hydroxyquinoline (C_9H_7NO, 8hq) was supplied from HiMedia Laboratories., and the reagents were analytical grade and were used without further purification.

2.2 Synthesis

2.2.1 Synthesis mesoporous silica (MCM)

In the beginning, the sodium silicate preparation was synthesized by silicon dioxide (SiO_2) from RH. The raw RH was boiled in 1 M HCl solution for 4 h, washed with distilled water, and then dried at 100 °C for 24 h. The dried RH was calcined in a muffle furnace, which was preheated to 900 °C, for 8 h (Bakar et al., 2016). Then, 100 mL of 2 M NaOH and 5 g of SiO_2 were stirring at 80-100 °C for 3 h. After the reaction period and cooling to room temperature the sodium silicate solution ($Na_2Si_3O_7$) formed was filtered and stored in a sealed

Suan Sunandha Science and Technology Journal

polypropylene flask at room temperature (Pimprom et al., 2015). Finally, the mesoporous silica was synthesized by the amount 0.8448 g of CTAB, 70.8 mL of deionized water, 800 mL of 99% methanol, and 29.2 mL of 28% aqueous ammonia were mixed and the mixture was stirred for 3 h at 20 °C. The 1.48 mL $Na_2Si_3O_7$ was added to the solution and then the suspensions were aged at 4 °C for another 24 h. The solid particles were collected by evaporation. The product was calcined in air at 660 °C for 10 h to form a porous silica shell. The molar ratio of MCM:C_{18}TAB:H_2O:NH_3:MeOH was 1:0.4:596:72:2993. (Kazuyuki et al., 201).

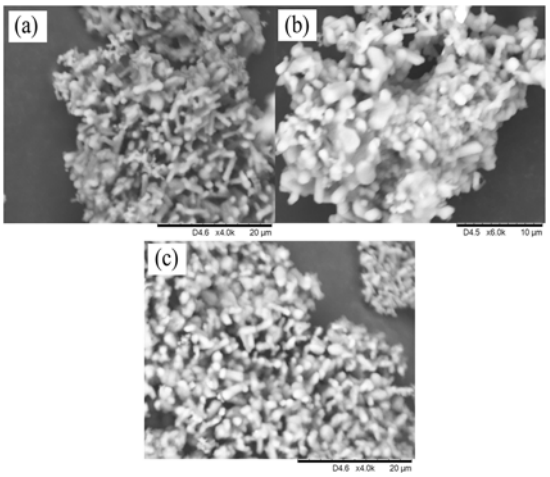

Figure 1. SEM images of MCM (a) MCM_Co(8hq)$_2$ (b) and MCMCo(II)_8hq (c)

2.2.2 Synthesis mesoporous silica (MCM)

The ligand cobalt complex-mesoporous silica hybrids were obtained by solid-state reaction at room temperature (Pimchan et al., 2014). The amount of Co(II) cation determined by atomic absorption spectrometry (AAS) was 0.0332 mg/g. The hybrids were obtained by two different processes as follows; the first method 0.1 g of mesoporous silica (MCM), 0.0305 g of $CoCl_2{\cdot}6H_2O$, and 0.0648 g of 8hq at the molar ratio of 1:2 for Co(II) to 8hq ligand were mixed ground in a agate mortar at room temperature for 10-15 min (MCM_Co(8hq)$_2$) and the another method was ground step by step, 0.1 g of mesoporous silica with 0.0305 g of $CoCl_2{\cdot}6H_2O$ were mixed ground in a agate mortar at room temperature for 10-15 min then add 0.0648 g of 8hq (the molar ratio 1:2 for Co(II):8hq ligand) mixed ground in a agate mortar at room temperature for 10-15 min respectively (MCMCo(II)_8hq).

2.3 Characterization

Material characterizations: A HITACHI TM 3000 scanning electron microscope (SEM) was used for the identification of morphology and size of nanoparticles. X-ray Powder Diffraction patterns (XRD) were obtained on a Bruker D8 ADVANCE diffractometer using monochromic Cu Kα radiation and Fourier-transform infrared spectroscopy (FTIR) was measured on a Spectrum One spectrometer over the spectral region of 600-4000 cm^{-1} by Bruker TENSOR27 confirmed the structural properties. The amount of metal ions were confirmed by atomic absorption spectrometry (AAS) on PinAAcle 900F Atomic absorption spectrometer. The result of optical properties by photoluminescence spectra were carried out from Spectrofluorometer FluoroMax 4 at the condition of a working voltage of 400 V and a slit width of 0.5 nm by the excitation of Xenon lamp at 320 nm.

3. Results and discussion

3.1 Mesoporous silica

The mesoporous silica was confirming the phase purity and identification through the SEM (Fig.1) and FT-IR (Fig.2). From the image (Fig.1) illustrated that the prominent morphology of particles is a mostly short rod-like cylinder and homogeneous aggregation of the particles is also observed. The diameters of particles approximately 1 μm and length up approximately 4 μm which is typically the morphology for mesoporous materials (Puratane & Amnuaypanich, 2018; Barczak, 2018; Cong, et al., 201). Figure 2. present the XRD patterns of mesoporous silica that the intensity of diffraction peaks at 2θ angles of 17.09°, 23.79°, 29.70°, 35.10°, 37.50°, 48.36° and 52.28° (JCPDS No. 16-0818), indicating that the crystalline phase of Na_2SiO_3 was the hexagonal phase (Li et al., 2019). The resulted of FT-IR spectrums demonstrate organic functional incorporation in silica framework (Fig.3) that the broad absorption band of 710 and 876 cm^{-1} corresponding Si-O-Si asymmetric bending and stretching respectively (Roschat et al., 2016), which were occurred from tetrahedral SiO_4 combination. The band due to 966 cm^{-1} shown stretching vibrations Si-OH (Yang et al., 2009; Yang et al., 2007; La-Salvia et al., 2017; Ogata, 2014). In addition, the absorption bands at 1428 cm^{-1} also corresponding Si=O formation (Roschat et, al. 2016) that the mesoporous silica morphology was confirmed.

Suan Sunandha Science and Technology Journal

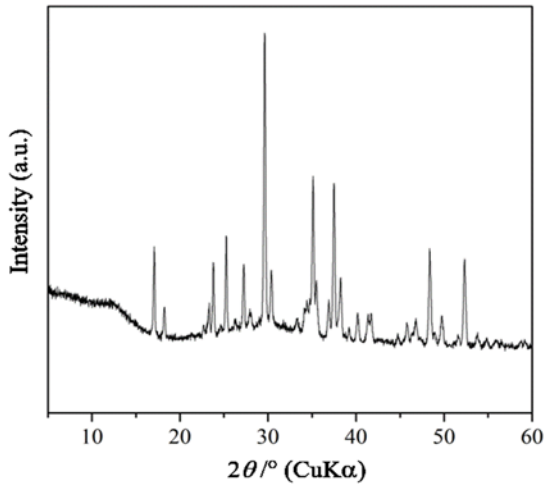

Figure 2. X-ray diffraction pattern of mesoporous silica from rice husk**.**

3.2 Bis(8-hydroxyquinoline)cobalt(II) into mesoporous silica

The preparation of the hybrid material of the cobalt (II) complex into mesoporous silica from the rice husk was confirmed by SEM, FT-IR and PL spectroscopies. Figure 1b. and 1c. showed the morphology after loading cobalt(II) complex into mesoporous silica from two different routes that the step by step ground product was obtained (Fig.1b) illustrated the microstructure was not changed from mesoporous silica (Fig. 1a). On the other hand, the hybrid material from mix ground method (Fig. 1c) was observed the little substances stuck on. The vibrations of CH_2 stretching as well as C-H vibration modes owing to the 8hq characteristics in $Co(8hq)_2$ and the FT-IR spectra of products are summarized in Figure 3. The absorption bands due to the C-H out of plane bending modes of the neat 8hq were observed at 815, 778, and 739 cm^{-1}, that all of the FT-IR spectra of the hybrids were shifted to higher frequencies were 820, 784 and 747 cm^{-1} for MCM_$Co(8hq)_2$ as well as the frequencies of MCMCo(II)_8hq at 820, 786 and 747 cm^{-1}, confirming the coordination between cobalt (II) cation and 8-hydroxyquinoline (Pimchan et al., 2014). The stretching vibrations of metal oxide for tetrahedrally coordinated Co(II) ions of both products were observed at 645 and 647 cm^{-1} respectively, indicating the formation of Co-O bonding in hybrid material (Li & Li, 2009; Saurav et al., 2015), supporting the interaction between hydroxyl group and cobalt(II) cation. A broad infrared absorption band in the region from 3000 to 3400 cm^{-1} identified the water of hydration in the samples (Li & Li, 2009), which was consistent with the photoluminescence spectra.

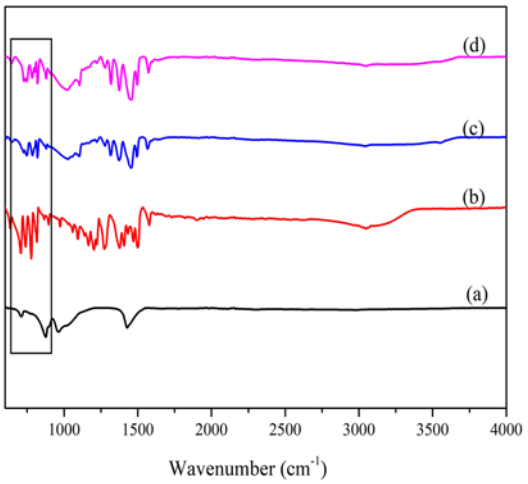

Figure 3. The FT-IR spectra of MCM (a), 8hq (b), MCM_$Co(8hq)_2$ (c) and MCMCo(II)_8hq (d)

Photoluminescence was a very important characteristic for the optical hybrid materials. All summaries were shown in Table 1. The luminescence spectrum of $Co(8hq)_2$ complex showed the emission band due to a π to π* charge transfer from the electron-rich phenoxide ring to the electron-deficient pyridyl ring of the ligand at 468 nm (Li & Li, 2009). When the product from a mixed ground method, the luminescence maxima was observed at 484 nm for MCM_$Co(8hq)_2$, as well as the color appearance was a dark green-orange (Fig.5b). In another route, the intense emission band of MCMCo(II)_8hq hybrids revealed at 474 nm and the feature observe as light-green (Fig.5c). The maxima luminescence spectra of MCMCo(II)_8hq (474 nm) was blue-shifted, while MCM_$Co(8hq)_2$ was demonstrated identical the maxima luminescence spectra as cobalt(II) complex (484 nm) in this comparison reflected the change in HOMO/LUMO level and/or bandgap energy of the interaction complexes (Pimchan et al., 2014), implying that the cobalt complex with different nanostructures or packing formed either of cobalt(II) complexes in the mesoporous silica spaces. For example, the photoluminescence of cobalt(II)-bis(8-hydroxyquinoline) nanosheets were red-shifted and the fluorescence quenching when the cobalt(II)complex formation between p-nitroaniline molecules (Li & Li, 2009). The emission peak of CA[n]@SiO_2@CdTe nanoparticles (NPs) was red-shifted in comparison with its precursor SiO_2@CdTe nanoparticles, which may be attributed to the increased size of nanoparticles (Li & Qu, 2007), while zinc(II)-bis(8-hydroxyquinoline)

Suan Sunandha Science and Technology Journal

complex in channels of mesoporous silica nanoparticles (MSN) which functionalized with or without mercapto groups, the PL emission peaks of these samples are red-shifted from 500 nm for MSN-Zn(8hq) to 511 nm for MSN-SH_2-Zn(8hq), the optical properties of these samples are dependent on the interior circumstances and the concentration of mercapto groups in channels of MSNs (Li et al., 2012). In addition, the reported that the emission peak maxima of nanoporous silica-Al(8hq)$_3$, nanoporous silica-Al(8hq)$_2$ and Al(8hq)$_3$ are 505, 497, and 510 nm respectively. The greater blue-shift was observed in the emission spectra of nanoporous silica-Al(8hq)$_2$ can be attributed to changing the coordination sphere of Al ions in nanoporous silica-Al(8hq)$_2$ in comparison with nanoporous silica-Al(8hq)$_3$ (Badiei & Goldooz, 2012). From these observations, the formation of cobalt complex into mesoporous silica were proved.

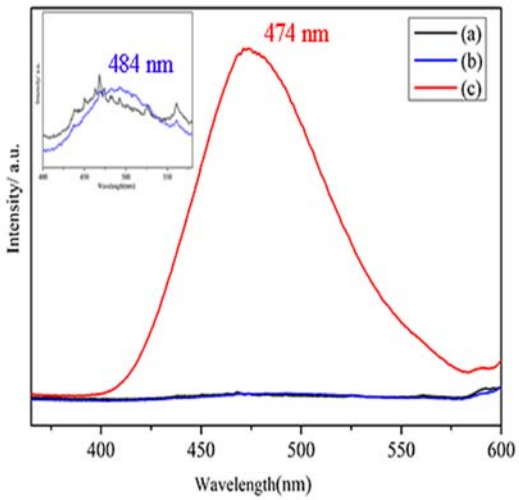

Figure 4. Luminescence spectra of Co(8hq)$_2$ (a), MCM_Co(8hq)$_2$ (b) and MCMCo(II)_8hq (c)

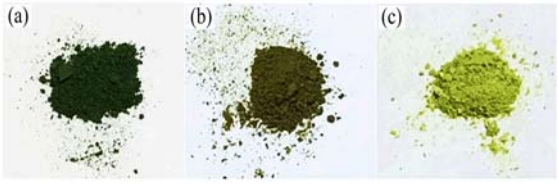

Figure 5. Colors of Co(8hq)$_2$ (a), MCM_Co(8hq)$_2$ (b) and MCMCo(II)_8hq (c)

In comparison of the luminescence efficiencies between MCM_Co(8hq)$_2$ and MCMCo(II)_8hq in Figure 4 demonstrates the excellence luminescence intensity of the hybrid material from step by step method (MCMCo(II)_8hq), while the other route product (MCM_Co(8hq)$_2$) modulate insignificantly from Co(8hq)$_2$ complex, indicating the sequenced ground direction be able to efficiently improve the luminescence intensity of metal complex (Pimchan et al., 2014). It was illustrated that the cobalt(II) complex of 8-hydroxyquinoline was successfully prepared into mesoporous silica via solid-state reaction at room temperature and the immobilized complexes into mesoporous silica exhibited excellent photoluminescence properties. Moreover, the method via step by step ground affected the molecular structure and/or packing of the complexes, which are thought to be correlated with the increased luminescence efficiencies. From these observations, the hybrids material showed the outstanding photoluminescence efficiencies as well as the shift of luminescence maxima due to the energy level changes (Pimchan et al., 2014).

Finally, the instant system is preparation of mesoporous silica, which conventional method and advantage rice husk. Applications such as the host material, absorbent, and insulator as well as the cobalt(II) complexes complement ruled by the mesoporous silica host. Suggestions for the incorporation of the other ligand metal complexes with different metal ions, ligands and/or other host structures are foreshadowing because of the ease of operation, the enhancement of luminescence efficiencies and the stability of the incorporated complexes.

4. Conclusions

The mesoporous silica which was synthesized by swelling-shrinking mechanism from rice husk was successfully prepared. The preparation of hybrid materials via solid-state reaction between mesoporous silica and cobalt(II) ion, as well as 8-hydroxyquinoline at the room temperature. The emission maxima was 484 nm for MCM_Co(8hq)$_2$ hybrid and 474 nm of MCMCo(II)_8hq hybrid. The photoluminescence efficiency of MCMCo(II)_8hq hybrid was higher than MCM_Co(8hq)$_2$, indicating that the MCMCo(II)_8hq hybrid constitute an excellent optical properties material. The difference in microstructure and/or packing of the cobalt(II) complex into mesoporous silica could be adjusted by a variant of loading/packing method. The solid-state reaction is applicable to prepare various complexes in the porous hosts.

Suan Sunandha Science and Technology Journal

5. Acknowledgment

Department of Chemistry, Faculty of Science and Technology and Science center, Rajabhat Maha Sarakham University for the facilities provided. Our also extends to gratitude Promotion of Science and Mathematics Talented Teachers (PSMT) for partial financial support.

References

Badiei, A., & Goldooz, H. (2012). A Simple Method for Preparation of Fluorescent Nanostructure Silica with Hexagonal Array. International *Journal of Modern Physics: Conference Series, 05*, 151-159. doi: 10.1142/S2010194512001961

Badiei, A., Goldooz, H., Ziarani, G. M., & Abbasi, A. (2011). One pot synthesis of functionalized SBA-15 by using an 8-hydroxyquinoline-5-sulfonamide-modified organosilane as precursor. *Journal of Colloid and Interface Science, 357*(1), 63-69. doi:10.1016/j.jcis.2011.01.049

Bakar, R. A., Yahya, R., & Gan, S. N. (2016). Production of High Purity Amorphous Silica from Rice Husk. *Procedia Chemistry, 19*, 189-195. doi:10.1016/j.proche.2016.03.092

Barczak, M. (2018). Functionalization of mesoporous silica surface with carboxylic groups by Meldrum's acid and its application for sorption of proteins. *Journal of Porous Materials, 26*(1), 291-300. doi:10.1007/s10934-018-0655-7

Behzad, S. K., Najafi, E., Amini, M. M., Janghouri, M., Mohajerani, E., & Ng, S. W. (2014). Yellow- green electroluminescence of samarium complexes of 8-hydroxyquinoline. *Journal of Luminescence, 156*, 219-228. doi:10.1016/j.jlumin.2014.08.013

Cong, V. T., Gaus, K., Tilley, R. D., & Gooding, J. J. (2018). Rod-shaped mesoporous silica nanoparticles for nanomedicine: recent progress and perspectives. *Expert Opinion on Drug, 15*(9), 881-892. doi:10.1080/17425247.2018.1517748

He, X., Yu, C., Lin, J., Zhang, X., Li, Q., Fang, Y.,… Tang, C. (2018). Porous boron nitride/rare earth complex hybrids with multicolor tunable photoluminescence. *Journal of Alloys and Compounds, 768*, 15-21. doi:10.1016/j.jallcom.2018.07.160

Jabariyan, S., & Zanjanchi, M. A. (2012). A simple and fast sonication procedure to remove surfactant templates from mesoporous MCM-41. *Ultrasonics Sonochemistry, 19*(5), 1087-1093. doi:10.1016/j.ultsonch.2012.01.012

Kudo, T., Ito, T., & Kim, S.-Y. (2017). Adsorption Behavior of Sr(II) from High-level Liquid Waste using Crown Ether with Ionic Liquid Impregnated Silica Adsorbent. *Energy Procedia, 131*, 189-194. doi:10.1016/j.egypro.2017.09.426

La-Salvia, N., Lovón-Quintana, J. J., Lovón, A. S. P., & Valença, G. P. (2017). Influence of Aluminum Addition in the Framework of MCM-41 Mesoporous Molecular Sieve Synthesized by Non-Hydrothermal Method in an Alkali-Free System. *Materials Research, 20*(6), 1461-1469. doi:10.1590/1980-5373-mr-2016-1064

Li, B., Li, H., Zhang, X., Fan, P., Liu, L., Li, B., … Zhao, B. (2018). Calcined sodium silicate as an efficient and benign heterogeneous catalyst for the transesterification of natural lecithin to L-α-glycerophosphocholine. *Green Processing and Synthesis, 8*, 78–84. doi:10.1515/gps-2017-0190

Li, F., Li, H., & Cui, T. (2017). One-step synthesis of solid state luminescent carbon-based silica nanohybrids for imaging of latent fingerprints. *Optical Materials, 73*, 459-465. doi:10.1016/j.optmat.2017.09.004

Li, H., & Li, Y. (2009). Synthesis of highly luminescent cobalt(II)-bis(8-hydroxyquinoline)nanosheets as isomeric aromatic amine probes. *Nanoscale*, *1*(1), 128-132. doi:10.1039/B9NR00019D

Li, H., & Qu, F. (2007). Selective inclusion of polycyclic aromatic hydrocarbons (PAHs) on calixarene coated silica nanospheres englobed with CdTe nanocrystals. *Journal of Materials Chemistry, 17*(33), 3536-3544. Doi: 10.1039/b705743a

Li, H., Fu, Y., Zhang, L., Liu, X., Qu, Y., Xu, S., & Lü, C. (2012). In situ route to novel fluorescent mesoporous silica nanoparticles with 8-hydroxyquinolinate zinc complexes and their biomedical applications. *Microporous and Mesoporous Materials,* 151, 293–302. doi:10.1016/j.micromeso.2011.10.021

Suan Sunandha Science and Technology Journal

Li, K.-M., Jiang, J.-G., Tian, S.-C., Chen, X.-J., & Yan, F. (2014). Influence of Silica Types on Synthesis and Performance of Amine-Silica Hybrid Materials Used for CO_2 Capture. *Physical Chemistry C, 118*(5), 2454-2462. doi:10.1021/jp408354r

Liu, Y., Wang, Z., Zeng, H., Chen, C., Liu, J., Sun, L., & Wang, W. (2015). Photoluminescent mesoporous carbon-doped silica from rice husks. *Materials Letters, 142,* 280-282. doi:10.1016/j.matlet.2014.12.034

Ma, J. S., Lin, L. Y., & Chen Y. S. (2019). Facile solid-state synthesis for producing molybdenum and tungsten co-doped monoclinic $BiVO_4$ as the photocatalyst for photoelectrochemical water oxidation. *International Journal of Hydrogen Energy, 44*(16), 7905-7914. doi:10.1016/j.ijhydene.2019.02.077

Maučec, D., Šuligoj, A., Ristić, A., Dražić, G., Pintar, A., & Tušar, N. N. (2018). Titania versus zinc oxide nanoparticles on mesoporous silica supports as photocatalysts for removal of dyes from wastewater at neutral pH. *Catalysis Today, 310*, 32-41. doi:10.1016/j.cattod.2017.05.061

Nakamura, K. J., Ide, Y., & Ogawa, M. (2011). Molecular recognitive photocatalytic decomposition on mesoporous silica coated TiO_2 particle. *Materials Letters, 65*(1), 24-26. doi:10.1016/j.matlet.2010.09.043

Ogata Y.H. (2018) *Characterization of Porous Silicon by Infrared Spectroscopy. In*: Canham L. (eds) Handbook of Porous Silicon. Springer, Cham.

Patel, V. K., Saurav, J. R., Gangopadhyay, K., Gangopadhyay, S., & Bhattacharya, S. (2015). Combustion characterization and modeling of novel nanoenergetic composites of Co_3O_4/nAl. *RSC Advances, 5*(28), 21471-21479. doi: 10.1039/c4ra14751k

Patriarca, M., Daier, V., Camí, G., Pellegri, N., Rivière, E., Hureau, C., & Signorella, S. (2019). Biomimetic Cu, Zn and Cu2 complexes inserted in mesoporous silica as catalysts for superoxide dismutation. *Microporous and Mesoporous Materials, 279*, 133-141. doi:10.1016/j.micromeso.2018.12.027

Pimchan, P., Khaorapapong, N., Sohmiya, M., & Ogawa, M. (2014). In situ complexation of 8-hydroxyquinoline and 4,4′-bipyridine with zinc(II) in the interlayer space of montmorillonite. *Applied Clay Science, 95*, 310-316. doi:10.1016/j.clay.2014.04.033

Pimprom, S., Sriboonkham, K., Dittanet, P., Föttinger, K., Rupprechter, G., & Kongkachuichay, P. (2015). Synthesis of copper-nickel/SBA-15 from rice husk ash catalyst for dimethyl carbonate production from methanol and carbon dioxide. *Journal of Industrial and Engineering Chemistry, 31*, 156-166. doi:10.1016/j.jiec.2015.06.019

Puratane, C. & Amnuaypanich, S. (2018). Mesoporous silica particles (MSPs) prepared by diol-functionalized natural rubber (ENR50-diol) and cationic surfactant (CTAB) dual templates, *KKU Sci. J. 46*(3), 496-505.

Rahman, A. Z. M. S. (2016). *Solid State Luminescent Materials: Applications. Reference Module in Materials Science and Materials Engineering.* doi:10.1016/b978-0-12-803581-8.04078-9

Roschat, W., Siritanon, T., Yoosuk, B., & Promarak, V. (2016). Rice husk-derived sodium silicate as a highly efficient and low-cost basic heterogeneous catalyst for biodiesel production. *Energy Conversion and Management, 119,* 453-462. doi:10.1016/j.enconman.2016.04.071

Sábio, R. M., Gressier, M., Caiut, J. M. A., Menu, M.-J., & Ribeiro, S. J. L. (2016). Luminescent multifunctional hybrids obtained by grafting of ruthenium complexes on mesoporous silica. *Materials Letters, 174*, 1-5. doi:10.1016/j.matlet.2016.03.058

Singh, D., Nishal, V., Bhagwan, S., Saini, R. K., & Singh, I. (2018). Electroluminescent materials: Metal complexes of 8-hydroxyquinoline-A review. *Materials & Design, 156*, 215-228. doi:10.1016/j.matdes.2018.06.036

Sohmiya, M., & Ogawa, M. (2011). Controlled spatial distribution of tris(2,2′-bipyridine)ruthenium cation ($[Ru(bpy)_3]^{2+}$) in aluminum containing mesoporous silicas. *Microporous and Mesoporous Materials, 142*(1), 363-370. doi:10.1016/j.micromeso.2010.12.023

Sohmiya, M., Saito, K., & Ogawa, M. (2015). Host-guest chemistry of mesoporous silicas: precise design of location, density and orientation of molecular guests in mesopores. *Science and Technology of Advanced Materials, 16*(5), 1-17. doi:10.1088/1468-6996/16/5/054201

Świderski, G., Kalinowska, M., Wilczewska, A. Z., Malejko, J., & Lewandowski, W. (2018). Lanthanide complexes with pyridinecarboxylic acids-Spectroscopic and thermal studies. *Polyhedron, 150*, 97-109. doi:10.1016/j.poly.2018.04.045

Tsuboi, T., Nakai, Y., & Torii, Y. (2012). Photoluminescence of bis(8-hydroxyquinoline) zinc (Znq_2) and magnesium (Mgq_2). *Open Physics, 10*(2). doi:10.2478/s11534-011-0090-8

Vibulyaseak, K., Deepracha, S., & Ogawa, M. (2018). Immobilization of titanium dioxide in mesoporous silicas; structural design and characterization. *Solid State Chemistry, 270*, 162-172. doi:10.1016/j.jssc.2018.09.043

Yang, J., Chen, J., & Song, J. (2009). Studies of the surface wettability and hydrothermal stability of methyl-modified silica films by FT-IR and Raman spectra. *Vibrational Spectroscopy, 50*(2), 178-184. doi:10.1016/j.vibspec.2008.09.016

Yang, P., Quan, Z., Lu, L., Huang, S., Lin, J., & Fu, H. (2007). MCM-41 functionalized with $YVO_4:Eu^{3+}$: a novel drug delivery system. *Nanotechnology, 18*(23), 1-10. doi:10.1088/0957-4484/18/23/235703

Zhang, X., Tang, J., Li, H., Wang, Y., Wang, X., Wang, Y., Huang, L., & Belfiore, L. A. (2018). Red light emitting nano-PVP fibers that hybrid with $Ag@SiO_2@Eu(tta)_3phen$-NPs by electrostatic spinning method. *Optical Materials, 78*, 220-225. doi:10.1016/j.optmat.2018.02.014

Zhao, H., Zhang, T., Qi, R., Dai, J., Liu, S., Fei, T., & Lu, G. (2017). Organic-inorganic hybrid materials based on mesoporous silica derivatives for humidity sensing. *Sensors and Actuators B: Chemical, 248*, 803-811. doi:10.1016/j.snb.2016.11.104

Available online at http://www.ssstj.sci.ssru.ac.th

SSSTJ

Suan Sunandha Science and Technology Journal

Numerical Approximations of Fredholm-Volterra Integral Equation of 2nd kind using Galerkin and Collocation Methods

Hasib Uddin Molla[1], Goutam Saha[1,*]

[1]Faculty of Science, Department of Mathematics, University of Dhaka, Dhaka 1000, Bangladesh

Corresponding author e-mail: *gsahamath@du.ac.bd

Received: *6 March 2020* / **Revised:** *26 March 2020* /**Accepted:** *31 March 2020*

Abstract

Galerkin and collocation approximation techniques are very effective and popular among researchers for numerical approximations of different types of differential, integral and integro-differential equations. Both methods approximate the solution by a finite sum of some known polynomials. In recent years, researchers around the world have been used different combinations of polynomials and collocation points in Galerkin and collocation methods for numerical approximations of different types of integral equations. Also, collocation method have been used more frequently compared to the Galerkin method. In this research, five different polynomials in Galerkin method and five different combinations of polynomials and collocation points in collocation method have been used for numerical approximations of linear FVIE of 2nd kind.It is found that the performances of different polynomials and collocation points in both these methods are consistent.

Keywords: Fredholm-Volterra integral equations, Galerkin method, collocation method, polynomials.

1. Introduction

There are mainly two classes of integral equations: Fredholm integral equation and Volterra integral equation. Both of these have linear and nonlinear forms. In this study, linear Fredholm-Volterra integral equations of 2nd kind are considered. Moreover, a similar study on Fredholm integral equation of 2nd kind is carried out by Molla and Saha, 2018.

There are several analytic methods and many approximation techniques available to solve different variations of integral equations. Among various approximation techniques, Galerkin and collocation methods are most popular and efficient, and they are also used to solve different versions of differential and integro-differential equations. In both Galerkin and collocation methods, unknown function is approximated by a finite sum of a set of known functions called as basis functions and such choice can be made from a wide variety of polynomials. Also, both of these methods follow different approaches to determine the expansion coefficients.

Fredholm-Volterra integral equations can be reduced to a system of algebraic equations by both Galerkin and collocation techniques. Yousuf and Razzaghi, 2005 used Legendre wavelets as the basis function in spectral method and then used zeroes of Chebyshev polynomials of first kind as the collocation points to solve nonlinear Fredholm-Volterra integral equations. Then Mandal and Bhattacharya, 2007 used Galerkin technique with Bernstein polynomials as basis functions for numerical approximate solutions of some classes of integral equations. Recently Hesameddini and Shahbazi, 2017 used Bernstein polynomials in spectral collocation method with Gauss-Legendre nodes as collocation points to solve system of Fredholm-Volterra integral equations. Shifted Chebyshev polynomials of 1st kind and roots of shifted Chebyshev polynomials of 1st kind are considered as basis and collocation points respectively by Dastjerdi and Ghaini, 2012 to solve linear FVIE. But at first, they transformed the FVIE by moving least square method and then applied spectral approximations. Wang and Wang, (2013, 2014) first transformed system of Fredholm-Volterra integral equations into matrix equations by collocation scheme where they used Lagrange's basis polynomials as the basis functions in the approximate solution. Later, they used Taylor polynomials as the basis in spectral method and

Suan Sunandha Science and Technology Journal

equally spaced nodes as collocation points and hence transformed the FVIE to matrix equation. Ebrahimi and Rashidinia, 2015 introduced a method for linear and nonlinear Fredholm and Volterra integral equations where approximate solution is collocated by cubic B-spline. Nemati, 2015 presented spectral method based on shifted Legendre polynomials and shifted Gauss Legendre nodes as collocation points for numerical approximation of the solution of Fredholm-Volterra integral equation. Also, Fibonacci polynomials and equally spaced nodes are used by Mirzaee and Hoseini, 2016 in spectral collocation method. More recently Liu et el., 2018 proposed a new spectral collocation technique where they used modified weighted Lagrange function known as barycentric Lagrange interpolation function along with Gauss-Lobatto nodes to solve linear high-dimensional Fredholm integral equations.

As far as our knowledge is concern, Galerkin method is used less frequently for Fredholm-Volterra integral equations and Bernstein polynomials are only used as basis functions. Then in collocation method, roots of Jacobi polynomials have not been considered yet for FVIE of 2nd kind.

In this study, Galerkin and collocation methods are considered for approximations of numerical solutions of linear Fredholm-Volterra integral equation of type II. Galerkin method is applied with five different polynomials: Legendre, Chebyshev 1st kind, Bernstein, Lagrange's and Fibonacci polynomials to observe their performance in numerical approximations of linear FVIE of type II. Numerical examples are used and results from each polynomial are compared with the available exact solution. Then collocation method is also applied with five different combinations of basis functions and collocation points and details are presented in Table 1. And hence the approximations are again compared with exact solution in each case. In each case collocation points are shifted in the required interval according to the numerical example.

Remaining portions of this article is presented as follows: In Section 1.1, brief introduction of polynomials and sets of collocation points are given. Then, details of formulation of system of linear algebraic equations from linear FVIE of 2nd kind using both Galerkin and collocation methods are given in Section 1.2. After that, numerical results of both the methods using different polynomials and collocation points are compared and resultant absolute errors are illustrated graphically in Section 1.3. Finally, in Section 1.4, a conclusion about this research is drawn.

Table 1. Combinations of polynomials and collocation points

Set of basis function	Collocation points
Chebyshev polynomials of 1st kind	Roots of Chebyshev polynomials of 1st kind
Legendre polynomials	Roots of Legendre polynomials
Bernstein polynomials	Roots of Jacobi polynomials
Lagrange's basis polynomials	Equally spaced nodes
Fibonacci polynomials	Gauss-Lobatto nodes

1.1 Introduction of polynomials and collocation points

In this section a very short introduction of Legendre, Chebyshev, Bernstein, Lagrange' s, Fibonacci and Jacobi polynomials are given. All these polynomials are being used frequently in approximations of the solution of various kinds of differential and integral equations. Techniques to generate collocation points for arbitrary interval $[a, b]$ from the roots of Legendre, Chebyshev and Jacobi polynomials; from the Gauss-Lobatto nodes and equally spaced nodes are presented.

Legendre polynomials**:** Legendre polynomials $P_i(w)$ are set of orthogonal polynomials over $[-1, 1]$ and are solutions of the Legendre differential equation.

We know that explicit formula for $P_i(w)$ is

$$P_i(w) = \sum_{k=0}^{i} \binom{i}{k}\binom{-i-1}{k}\left(\frac{1-w}{2}\right)^k, i = 0,1,2 \dots$$

And, the recurrence relation for Legendre polynomials are as follows**:**

$$P_0(w) = 1, P_1(w) = w$$
$$(i+1)P_{i+1}(w) = (2i+1)wP_i(w) - iP_{i-1}(w),$$
$$i = 1,2, \dots$$

The roots of the Legendre polynomials are in the interval $(-1, 1)$. In order to generate set of collocation points

$$LCP = [x_k]_{k=0}^{k=n}$$

over the interval $[a, b]$, the following points along with $x_0 = a$ and $x_n = b$ are considered.

$$x_k = \frac{b-a}{2} + \frac{b-a}{2} w_k \ ; k = 1,2,..,n-1$$

where w_k is a root of the Legendre polynomials $P_{n-1}(w)$ with $w_k < w_{k+1}$ for $k = 1, 2, \dots, n-2$.

Suan Sunandha Science and Technology Journal

Chebyshev polynomials**:** Chebyshev polynomials of first kind $T_i(y)$ are set of orthogonal polynomials over $[-1,1]$ and are solutions of the Chebyshev differential equation. We know that explicit formula for $T_i(y)$ is

$$T_i(y) = y^i \sum_{k=0}^{\left\lfloor \frac{i}{2} \right\rfloor} \binom{i}{2k} (1-y^{-2})^k, i = 0,1,2, \ldots.$$

And, the recurrence relation for Chebyshev polynomials of first kind are as follows**:**

$$T_0(y) = 1, T_1(y) = y$$
$$T_{i+1}(y) = 2yT_i(y) - T_{i-1}(y), i = 1,2, \ldots$$

Like Legendre polynomials, roots of the Chebyshev polynomials are in the interval $(-1,1)$. In order to generate set of collocation points

$$CCP = [x_k]_{k=0}^{k=n}$$

over the interval $[a,b]$, following points along with $x_0 = a$and $x_n = b$ are considered.

$$x_k = \frac{b-a}{2} + \frac{b-a}{2} y_k \ ; k = 1,2,..,n-1$$

where y_k are the roots of the Chebyshev polynomials $T_{n-1}(y)$ with $y_k < y_{k+1}$ for $k = 1,2,\ldots,n-2$.

Bernstein polynomials**:** The i[th] degree Bernstein polynomials defined on the interval $[a,b]$ are

$$B_{r,i}(y) = \binom{i}{r} \frac{(y-a)^r (b-y)^{i-r}}{(b-a)^i} \ ; \ a \le y \le b,$$
$$r = 0,1,2, \ldots, i$$

where

$$\binom{i}{r} = \frac{i!}{r!\,(i-r)!}$$

There are $(i+1)$ Bernstein polynomials of i[th] degree with following properties**:**

$$B_{r,i}(y) = 0, if r < 0 \ or r > i$$
$$B_{r,i}(a) = B_{r,i}(b) = 0 \ , 1 \le r \le i-1$$

Lagrange basis polynomials**:** With $(n+1)$ points $x_0, x_1, x_2, \ldots\ldots, x_{n-1}, x_n$, Lagrange basis polynomials $L_i(x); i = 0,1,2, \ldots, n$ are defined by

$$lp(x) = \prod_{r=0}^{n} (x - x_r)$$

$$L_i(x) = \frac{lp(x)}{lp'(x)(x-x_i)} \quad ; i = 0,1,2, \ldots, n$$

with the property $L_i(x_j) = \delta_{ij}$, where $\delta_{ij}$is the Kronecker delta function. Here $lp'(x)$ is the derivative of $lp(x)$.

Fibonacci polynomials**:** Fibonacci polynomials are set of polynomials $F_i(u)$ defined by

$$F_i(u) = \sum_{k=0}^{\left\lfloor \frac{i}{2} \right\rfloor} \binom{i-k}{k} u^{i-2k}, \quad i = 0,1,2, \ldots$$

And, the recurrence relation for Fibonacci polynomials are follows**:**

$$F_0(u) = 1, F_1(u) = u$$
$$F_{i+1}(u) = uF_i(u) + F_{i-1}(u), \ i = 1,2,3, \ldots$$

Jacobi polynomials**:** Jacobi polynomials $P_i^{\alpha,\beta}(y)$ are set of orthogonal polynomials on the interval $[-1,1]$ with respect to the weight function $(1-y)^\alpha (1+y)^\beta$. Roots of Jacobi polynomials are lies in the interval $(-1,1)$. Hence, to generate set of collocation points

$$JCP = [x_k]_{k=0}^{k=n}$$

over the interval $[a,b]$, the following points along with $x_0 = a$ and $x_n = b$ are considered:

$$x_k = \frac{b-a}{2} + \frac{b-a}{2} y_k \ ; k = 1,2,..,n-1$$

where y_k are the roots of the Jacobi polynomials $P_{n-1}^{1,1}(y)$ with $y_k < y_{k+1}$for $k = 1,2, \ldots, n-2$ and

$$P_i^{\alpha,\beta}(y) = \frac{\Gamma(\alpha+i+1)}{i!\ \Gamma(\alpha+\beta+i+1)}$$
$$\sum_{m=0}^{i} \binom{i}{m} \frac{\Gamma(\alpha+\beta+i+m+1)}{\Gamma(\alpha+m+1)} \left(\frac{y-1}{2}\right)^m$$

Gauss**-**Lobatto nodes**:** In order to generate set of collocation points

$$GLCP = [x_k]_{k=0}^{k=n}$$

over the interval $[a,b]$, let us consider:

$$x_k = \frac{b-a}{2} + \frac{b-a}{2} \cos\frac{k\pi}{n} \ ; k = 0,1,2,..,n$$

Equally spaced nodes**:** In order to generate set of collocation points

$$ESCP = [x_k]_{k=0}^{k=n}$$

from equally spaced nodes over the interval $[a,b]$, following points are considered:

$$x_k = a + k\frac{b-a}{n} \ ; k = 0,2, \ldots, n$$

1.2 Solution procedure for linear FVIE

All integral equations can describe various physical phenomena, scientific and engineering problems. Linear Fredholm-Volterra integral equations of 2[nd] kind arises from different types of

Suan Sunandha Science and Technology Journal

differential equations and can be described in many physical phenomena which have scientific interests. Here we consider the following general form of linear Fredholm-Volterra integral equation of 2nd kind:

$$\phi(x) + \lambda_1 \int_a^b k_1(x,t)\phi(t)dt + \lambda_2 \int_a^x k_2(x,t)\phi(t)dt = f(x), \quad a \le x \le b \qquad (1)$$

where $k_1(x,t), k_2(x,t)$ and $f(x)$ are known functions, λ_1 and λ_2 are known parameters, and $\phi(x)$ is the unknown solution of Eq. (1), needed to be resolved.

To approximate the solution $\phi(x)$ of Eq. (1) using Galerkin and collocation methods, first let's, consider the following form of the trial solution $\tilde{\phi}(x)$:

$$\tilde{\phi}(x) = \sum_{i=0}^{n} m_i Q_i(x) \qquad (2)$$

Here $Q_i(x)$ are called as basis functions and generally some known polynomials are used as basis function. In trial solution, m_i are the unknown parameters also known as expansion coefficients. Using the trial solution from Eq. (2) into Eq. (1), we can have

$$\sum_{i=0}^{n} m_i Q_i(x) + \lambda_1 \int_a^b k_1(x,t) \sum_{i=0}^{n} m_i Q_i(t)\,dt + \lambda_2 \int_a^x k_2(x,t) \sum_{i=0}^{n} m_i Q_i(t)\,dt = f(x)$$

$$\Rightarrow \sum_{i=0}^{n} m_i \left[Q_i(x) + \lambda_1 \int_a^b k_1(t,x)Q_i(t)dt + \lambda_2 \int_a^x k_2(t,x)Q_i(t)dt \right] = f(x) \qquad (3)$$

To determine the expansion coefficients by Galerkin method, first multiply Eq. (3) by $Q_j(x)$ and then integrate with respect to x from a to b. Thus Eq. (3) reduces to

$$\sum_{i=0}^{n} m_i \left[\int_a^b \left[Q_i(x) + \lambda_1 \int_a^b k_1(t,x)Q_i(t)dt + \lambda_2 \int_a^x k_2(t,x)Q_i(t)dt \right] Q_j(x)dx \right] = \int_a^b f(x)Q_j(x)dx\,; \quad j = 0,1,..,n$$

This is equivalent to the following linear system of equations:

$$\sum_{i=0}^{n} m_i R_{i,j} = F_j\,, j = 0,1,2,\dots,n \qquad (4)$$

where

$$R_{i,j} = \int_a^b \left[Q_i(x) + \lambda_1 \int_a^b k_1(t,x)Q_i(t)dt + \lambda_2 \int_a^x k_2(t,x)Q_i(t)dt \right] Q_j(x)dx\,;$$

$$F_j = \int_a^b f(x)Q_j(x)\mathrm{dx}\ , i,j = 0,1,2,\dots,n$$

System of linear equations in Eq. (4) is called the Galerkin equation and by solving Eq. (4), the expansion coefficients m_i can be determined easily.

In collocation method, to determine expansion coefficients m_j, chose a point x_j in the domain for each m_j in the trial solution. These points x_j are known as collocation points. Then forcing Eq. (3) to satisfy at each x_j yields

$$\sum_{i=0}^{n} m_i \left[Q_i(x_j) + \lambda_1 \int_a^b k_1(t,x_j)Q_i(t)dt + \lambda_2 \int_a^x k_2(t,x_j)Q_i(t)dt \right] = f(x_j)\,; \qquad (5)$$

$j = 0,1,2,\dots,n$

Thus, a trial solution with $(n+1)$ unknown parameters produce following linear system of equations:

$$\sum_{i=0}^{n} m_i G_{i,j} = H_j\ ; \quad j = 0,1,2,\dots,n \qquad (6)$$

where

Suan Sunandha Science and Technology Journal

$$G_{i,j} = Q_i(x_j) + \lambda_1 \int_a^b k_1(t, x_j) Q_i(t) dt + \lambda_2 \int_a^x k_2(t, x_j) Q_i(t) dt ;$$

$$H_j = f(x_j), \quad i, j = 0,1,2, \dots, n$$

System of linear equations in Eq. (6) is called the collocation equation and by solving Eq. (6), the expansion coefficients m_i can be determined. So, once the set of basis functions $\{Q_i\}_{i=0}^n$ is chosen then based on Galerkin or collocation approach, expansion coefficients m_i can be found using Eqs. (4) or (6). And then substituting these values into Eq. (2) will give the approximate solution of FVIE of type II in terms of finite sum of series of functions $\{Q_i\}_{i=0}^n$.

1.3 Results and discussion

This research is performed to compare the performance of different polynomials in Galerkin method and different combinations of polynomials and sets of collocation points in collocation method for numerical approximations of linear Fredholm-Volterra integral equation of 2nd kind. Followings are the list of polynomials and combinations used for these two methods:

Table 2. Sets of basis and collocation points for both methods

Galerkin	**Collocation**	
Set of basis	Set of basis	Set of collocation points
$\{P_i\}_{i=0}^n$	$\{P_i\}_{i=0}^n$	LCP
$\{T_i\}_{i=0}^n$	$\{T_i\}_{i=0}^n$	CCP
$\{B_{i,n}\}_{i=0}^n$	$\{B_{i,n}\}_{i=0}^n$	JCP
$\{L_i\}_{i=0}^n$	$\{L_i\}_{i=0}^n$	$ESCP$
$\{F_i\}_{i=0}^n$	$\{F_i\}_{i=0}^n$	$GLCP$

With $n = 5$, five sets of collocation points for the interval $[0,1]$ are as follows:

Table 3. Sets of collocation points for $n = 5$

LCP	{0, 0.0694318, 0.330009, 0.669991, 0.930568, 1}
CCP	{0, 0.0380602, 0.308658, 0.691342, 0.96194, 1}
JCP	{0, 0.117472, 0.357384, 0.642616, 0.882528, 1}
$ESCP$	{0, 0.2, 0.4, 0.6, 0.8, 1}
$GLCP$	{0, 0.0954915, 0.345492, 0.654508, 0.904508, 1}

Here two numerical examples are considered to carry out the investigations and in both examples domain of the problem is $[0,1]$.

Example 1: Consider the following example of linear FVIE of 2nd kind:

$$\phi(x) + \int_0^1 e^{x+t}\phi(t)dt - \int_0^x e^{x+t}\phi(t)dt = e^{-x} - (x-1)e^x, \quad 0 \le x \le 1$$

Exact solution of this problem is $\phi(x) = e^{-x}$.

At first, the performance of Legendre, Chebyshev, Bernstein, Lagrange's and Fibonacci polynomials are observed in Galerkin method for this problem. Absolute errors of example 1 in Galerkin method for five sets of basis functions given in Table 2 with $n = 5$ are presented in Fig. 1.

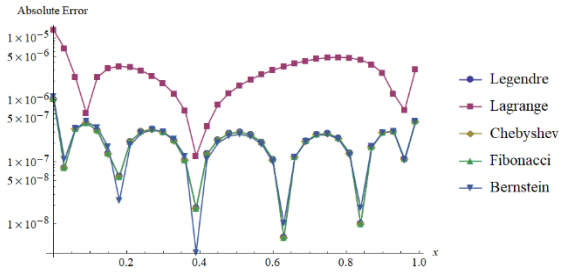

Figure 1: Absolute error curves of example 1 in Galerkin method

Now, performance of different combinations of polynomials and set of collocation points are observed in collocation method. Numerical solutions of example 1 in collocation method with different combinations given in Table 2 with $n = 5$ are given in the Table 4 and corresponding absolute error curves are presented in Fig. 2.

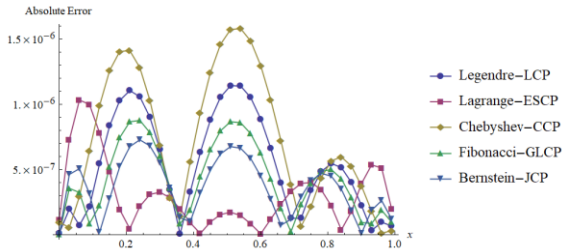

Figure 2:Absolute error graphs of example 1 in collocation method

Example 2: Consider the following example of linear FVIE of 2nd kind used by Wang and Wang, 2013:

$$\phi(x) + \int_0^1 e^t \sin x\, \phi(t)dt - \int_0^x e^t \cos x\, \phi(t)dt = f(x), \quad 0 \le x \le 1$$

where

$$f(x) = e^x - \frac{1}{2}(e^{2x} - 1)\cos x + \frac{1}{2}(e^2 - 1)\sin x$$

Suan Sunandha Science and Technology Journal

Exact solution of this problem is $\phi(x) = e^x$

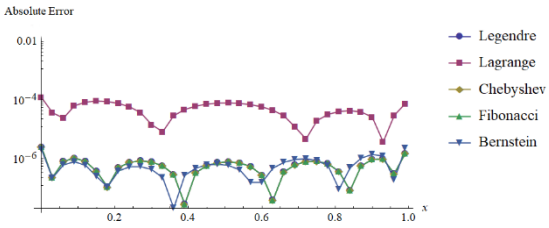

Figure 3: Absolute error curves of example 2 in Galerkin method

Like the previous example, at first, the performance of Legendre, Chebyshev, Bernstein, Lagrange's and Fibonacci polynomials are observed in Galerkin method for this problem. Absolute errors of example 2 in Galerkin method for five sets of basis given in Table 2 with $n = 5$ are presented in Fig. 3.

Now, performance of different combinations of polynomials and set of collocation points are observed in collocation method. Numerical solutions of example 2 in collocation method with different combinations given in Table 2 with $n = 5$ are also given in Table 5 and corresponding absolute error curves are presented in Fig. 4.

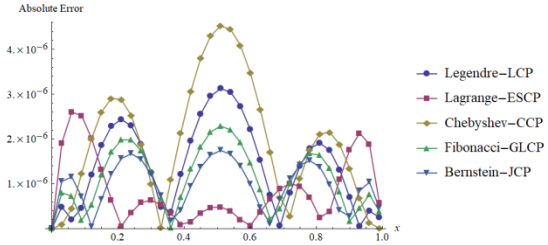

Figure 4: Absolute error graphs of example 2 in collocation method

After investigation of the absolute errors of both examples in Galerkin method, it is evident that Legendre, Chebyshev, Fibonacci and Bernstein polynomials give better solution than Lagrange's polynomial whereas solutions from first three polynomials are almost the same. Though there are some variations between solutions from Bernstein and Legendre, Chebyshev and Fibonacci but no clear conclusion can be made about the performance of the polynomials. In collocation method, performance of different combinations of basis functions and collocation point's sets are consistent in both problems. Lagrange's polynomials with ESCP handle the errors better than the others except around the both boundaries. Among rest of the combinations, overall performance of Bernstein & JCP, Fibonacci & GLCP, Legendry & LCP and Chebyshev& CCP follows the downward trend.

1.4 Conclusion

In this article, formulation of system of linear algebraic equations for linear FVIE of 2nd kind by both Galerkin and collocation methods are presented to determine the expansion coefficients. Then five different polynomials: Legendre, Chebyshev, Fibonacci, Bernstein and Lagrange's are being used in Galerkin method. In both test problems, it is found that first four polynomials give better solution than Lagrange's polynomials. It is also noticed that in Galerkin method, Legendre, Chebyshev and Fibonacci polynomials give the same solutions. In collocation method, five different combinations of polynomials and collocation points are being tried. All the combinations produced very good approximations. Lagrange's polynomials and ESCP performed well compared to the others followed by Bernstein and JCP and performance of Chebyshev polynomials and CCP are worst.

Conflict of Interest

The authors do not report any financial or personal connections with other persons or organizations, which might negatively affect the contents of this publication and/or claim authorship rights to this publication.

Publication Ethic

Submitted manuscripts must not have been previously published by or be under review by another print or online journal or source.

References

Dastjerdi, H. L. & Ghaini, F. M. M. (2012). Numerical solution of Volterra- Fredholm integral equations by moving least square method and Chebyshev polynomials. *Applied Mathematics Modelling*, 36, 3283-3288.doi:10.1016/j.apm.2011.10.005

Ebrahimi, N. & Rashidinia, J. (2015). Collocation method for linear and nonlinear Fredholm and Volterra integral equations. *Applied Mathematics and Computation*, 270, 156-164.doi: 10.1016/j.amc.2015.08.032

Suan Sunandha Science and Technology Journal

Hesameddini, E. & Shahbazi, M. (2017). Solving system of Volterra- Fredholm integral equations with Bernstein polynomials and hybrid Bernstein block- pulse functions. *Journal of Computational and Applied Mathematics*, 315, 182- 194. doi: 10.1016/j.cam.2016.11.004

Liu, H., Huang, J., Pan, Y. & Zhang, J. (2018). Barycentric interpolation collocation methods for solving linear and nonlinear high-dimensional Fredholm integral equations. *Journal of Computational and Applied Mathematics*, 327, 141- 154. doi: 10.1016/j.cam.2017.06.004

Mandal, B. N. & Bhattacharya, S. (2007). Numerical solution of some classes of integral equations using Bernstein polynomials. *Applied Mathematics and Computation*, 190, 1707-1716.doi: 10.1016/j.amc.2007.02.058

Mirzaee, F. & Hoseini, S. F. (2016). Application of Fibonacci collocation method for solving Volterra-Fredholm integral equations. *Applied Mathematics and Computation*, 273, 637-644.doi: 10.1016/j.amc.2015.10.035

Molla, H. U. & Saha, G. (2018). Numerical approximation of Fredholm integral equation (FIE) of 2nd kind using FE- Galerkin and collocation methods. *GANIT: Journal of Bangladesh Mathematical Society*, 38,11-25.doi:10.3329/ganit.v38i0.39782

Nemati, S. (2015). Numerical solution of Volterra-Fredholm integral equations using Legendre collocation method. *Journal of Computational and Applied Mathematics*, 278, 29- 36. doi: 10.1016/j.cam.2014.09.030

Wang, K. & Wang, Q. (2013). Lagrange collocation method for solving Volterra-Fredholm integral equations. *Applied Mathematics and Computation*, 219, 10434- 10440. doi: 10.1016/j.amc.2013.04.017

Wang, K. & Wang, Q. (2014). Taylor collocation method and convergence analysis for the Volterra-Fredholm integral equations. *Journal of Computational and Applied Mathematics*, 260, 294-300.doi: 10.1016/j.cam.2013.09.050

Yousuf, S. & Razzaghi, M. (2005). Legendre wavelets method for the nonlinear Volterra-Fredholm integral equations. *Mathematics and Computers in Simulation*, 70, 1- 8. doi: 10.1016/j.matcom.2005.02.035

Suan Sunandha Science and Technology Journal

Appendix: A

Table 4. Solutions of example 1 in collocation method

x	Exact	Legendre-LCP	Chebyshev-CCP	Bernstein-JCP	Lagrange-ESCP	Fibonacci-GLCP
0.	1.000000000	0.999999986	0.999999903	0.999999998	0.999999881	1.000000005
0.1	0.904837418	0.904837092	0.904836653	0.904837641	0.904838360	0.904837405
0.2	0.818730753	0.818729658	0.818729327	0.818730116	0.818730779	0.818729914
0.3	0.740818221	0.740817567	0.740817534	0.740817669	0.740817892	0.740817617
0.4	0.670320046	0.670320480	0.670320739	0.670320224	0.670319988	0.670320325
0.5	0.606530660	0.606531784	0.606532207	0.606531326	0.606530834	0.606531513
0.6	0.548811636	0.548812524	0.548812934	0.548812086	0.548811627	0.548812264
0.7	0.496585304	0.496585344	0.496585583	0.496585121	0.496584944	0.496585206
0.8	0.449328964	0.449328427	0.449328428	0.449328497	0.449328692	0.449328457
0.9	0.406569660	0.406569434	0.406569283	0.406569672	0.406570054	0.406569563
1	0.367879441	0.367879441	0.367879441	0.367879441	0.367879441	0.367879441

Table 5. Solutions of example 2 in Galerkin method

x	Exact	Legendre-LCP	Chebyshev-CCP	Bernstein-JCP	Lagrange-ESCP	Fibonacci-GLCP
0.	1.000000000	1.000000000	1.000000000	1.000000000	1.000000000	1.000000000
0.1	1.105170918	1.105170213	1.105169417	1.105171419	1.105173304	1.105170874
0.2	1.221402758	1.221400338	1.221399830	1.221401287	1.221402990	1.221400838
0.3	1.349858808	1.349857556	1.349857808	1.349857597	1.349858176	1.349857533
0.4	1.491824698	1.491826169	1.491827164	1.491825292	1.491824689	1.491825620
0.5	1.648721271	1.648724368	1.648725755	1.648723001	1.648721761	1.648723539
0.6	1.822118800	1.822121010	1.822122279	1.822119788	1.822118734	1.822120264
0.7	2.013752707	2.013752392	2.013753071	2.013751894	2.013751763	2.013752061
0.8	2.225540928	2.225539027	2.225538900	2.225539481	2.225540514	2.225539247
0.9	2.459603111	2.459602416	2.459601769	2.459603380	2.459604871	2.459602945
1	2.718281828	2.718281822	2.718281707	2.718281828	2.718281631	2.718281844

Available online at http://www.ssstj.sci.ssru.ac.th

SSSTJ

Suan Sunandha Science and Technology Journal

GIS-based site analysis for selecting suitable sites of waste-to-energy plants in Pathumthani

Vivian Chullamon[1*], Wanwisa Skolpap[2]

[1] Department of Chemical Engineering, School of Engineering, Thammasat University (Rangsit campus), [1] Pathumthani, 12120, Thailand

[2] Department of Chemical Engineering, Center of Clinical Engineering, School of Engineering, Thammasat University (Rangsit campus), Pathumthani, 12120, Thailand

Corresponding author e-mail: * vivianteve@gmail.com

Received: *5 March 2020* / **Revised:** *5 May 2020* / **Accepted:** *20 May 2020*

Abstract

In response to cumulative municipal waste problem in Pathumthani, a waste-to-energy electric power plant is selected as waste management approach. This study aims at assessing waste-to-energy power plant potential zones in Pathumthani using Geographic Information System (GIS). GIS data collection depends on all 12 factors considered in this study as follows: the distances from power plant site to communities, to industrial areas, to power lines, to power stations, to waterworks stations, to hospitals, to education institutes, to main water resources, to accessible roads, to railways, to airports and the risk of flooding. After multiple layers of information have been generated as a single map using GIS, the suitable power plant locations are defined on the basis of the ordered weighted averaging (OWA) technique. Color-coded symbology is applied to the maps to differentiate suitable/unsuitable areas for power plant establishment. Considering proportions of suitable areas of each of the seven districts to the total area of the province, the most suitable district is Klong Luang, followed by Nongsua, Lamlukka, Ladlumkaew, Muang Pathumthani, Thanyaburi, and Samkok districts, respectively. This analysis approach should be further developed and applied to other areas.

Keywords: Waste-to-energy power plant, Location suitability analysis, Pathumthani, GIS

1. Introduction

The domestic disposal of municipal solid waste is inappropriate such as uncontrolled incineration and open dumping leading to difficulties in recycling programs. These open-air disposal approaches cause hazardous air pollution associated with PM 2.5 exposure. According to the Waste Management Master Plan of Thailand (2016-2021), the sustainable reginal solid waste management in Thailand has planned to launch proper recycling project by 2021. Therefore, government and private sectors need to make implement the waste management technology.

Several big cities in Thailand are currently facing problems concerning a large quantity of garbage. Therefore, efficient garbage management solutions are required. One promising outcome relies on a conversion of garbage into electricity as the benefit of this strategy. In this case, Pathumthani, a metropolitan area, is a fast−growing city with continuously increasing number of population, resulting in increasing daily amount of waste. Pathumthani handles approximately 1,829 tons of garbage per day. About 70% of this amount is disposed in nearby provinces while the remaining 30% accumulates daily within the province. The management of substantial quantity of accumulated wastes is endorsed by central government policy for energy recovered from municipal solid wastes in different regions including Pathumthani. Criterion for siting a suitable solid waste incineration power plant is considered not only appropriate location, but also optimal one to avoid unnecessary loss caused by unexpected disaster and public dissatisfaction. Site selection for the waste−to−energy plant in Pathumthani, one of influencing factors is the region specified as the area for raw water source conservation for Metropolitan Waterworks Authority. A raw water pumping station located in Muang district in Pathumthani extracts raw water from the Chao Phraya River to produce and distribute tap water to eastern part of Bangkok.

Suan Sunandha Science and Technology Journal

Therefore, the result of suitability assessment for site selection of waste−to−energy power plant should be satisfied by all stakeholders.

This research conducted to evaluate potential site of waste−to−energy power plant for a moving grate incineration of solid waste in Pathumthani limits the scope of this investigation. The moving grate incineration technology is selected as energy recovery from municipal solid waste owing to less electricity consumption required for reduction of large waste volume. Selecting a possible location for construction of waste−to−energy plant in Pathumthani via geographic information system (GIS) analysis is applied by ranking of the area based on their weighted suitability score assigned to each factor such as distance to water sources, distance to electricity systems, distance to public water supply systems, distance to roads, and distance to the residential and etc. (Misra & Sharma, 2015). A decision making tool for suitability analysis of potential sites is geographic information system (GIS) due to its high capacity in collecting, displaying, and analyzing multiple datasets (Rikalovic, Cosic, & Lazarevic, 2014). The application of GIS and spatial data provided a set of attribute values is efficient for assessing potential candidate sites to construct waste−to−energy power plants based on the suitability score (Goyal, Sharma, & Joshi, 2017). The decision−making approach in site selection for waste−to−energy power plant in Pathumthani is the integration of Ordered Weighted Averaging (OWA) technique with GIS that the order weights assigned to a given criteria for all factors according to specific requirements and preferences are taken into account (Zahibi, et al., 2019).

2. Research objectives

1. To specify factors and criteria for selecting suitable locations of waste-to-energy power plants in Pathumthani based on GIS data

2. To determine appropriate sites of waste-to-energy power plants in Pathumthani using the Ordered Weighted Averaging technique

3. Methodology

The research methodology can be divided into two parts namely the part of data collection and the part of GIS-based data analysis as described below.

3.1 Data collection for each factor

This research has collected data of influencing on suitability of waste-to-energy power plant sites from three main governmental organizations namely Department of Public Works and Town & Country Planning (DPT), Provincial Electricity Authority (PEA), and Provincial Waterworks Authority (PWA). Based on the acquired data, there were 12 factors for assessing site suitability using the selected criteria by environmental experts for assigning weights and scores as shown in Table 1.

Table 1. List of decision factors and their associated criteria, weights, and scores for suitability analysis of waste−to−energy power plant sites

No.	Analyzed factors (variables)	Criteria	Weight	Score	Data source
1	Distance from urban areas and community centers	Over 5 km away from communities	15	3	Using munisan_a dataset of DPT
		3-5 km away from communities		2	
		< 3 km from communities		1	
2	Distance from industrial areas	< 0 km from industrial areas	10	3	Extracting features with codes 3000-3800 from Landsum_a dataset of DPT
		1-3 km away industrial areas		2	
		Over 3 km away from industrial areas		1	
3	Distance from power lines	< 50 m from power lines	10	3	Using LB_Centertline dataset of PEA
		50-100 m from power lines		2	
		Over 100 m from power lines		1	
4	Distance from power stations	< 50 m from power stations	12	3	Using DS_T_Station dataset of PEA
		50-100 m from power stations		2	

Suan Sunandha Science and Technology Journal

No.	Analyzed factors (variables)	Criteria	Weight	Score	Data source
		Over 100 m from power stations		1	
5	Distance from waterworks stations	Over 100 m from waterworks	12	3	Merging district-level data of PWA to derive PWA_merged dataset
		50-100 m from waterworks		2	
		< 50 m from waterworks		1	
6	Distance from hospitals	Over 5 km away from hospitals	7	3	Extracting features with codes 6500-6580 from Landsum_a dataset of DPT
		2-5 km from hospitals		2	
		0-2 km from hospitals		1	
		Overlapping hospitals		0	
7	Distance from education institutes (academies)	Over 3 km away from academies	6	3	Extracting features with codes 6100-6180 from Landsum_a dataset of DPT
		1-3 km from academies		2	
		0-1 km from academies		1	
		Overlapping academies		0	
8	Distance from main water resources	Over 1 km away from water resources	12	3	Extracting features with codes 9511 (rivers) and 9512 (canals) from Landsum_a dataset of DPT
		0.5-1 km from water resources		2	
		10 m - 0.5 km from water resources		1	
		Overlapping or within 10 m from water resources		0	
9	Accessible roads	3-300 m away from roads	7	3	Using roadedge_a dataset of DPT
		300-800 m from roads		2	
		Over 800 m away from roads		1	
		Overlapping or within 3 m from roads		0	
10	Flood risk levels	Low level of flood risk	9	3	Using F-DWR2 dataset of Department of Water Resources
		Moderate level of flood risk		2	
		High level of flood risk		1	
11	Railways	Overlapping railways or within 20 m away from railways	0	0	Using railedge_a dataset of DPT
12	Airports	Overlapping airport areas	0	0	Using airport_a dataset of DPT
		Total weight	**100**		

Note: The factors and their criteria weights, and scores were derived from relevant literatures and communication with domain experts.

3.2 Data analysis procedures

The data analysis consists of the following procedures.

a. Make the dataset of each factor containing distance information according to the specified criteria by using the Multiple Ring Buffer command of ArcGIS and editing the output attribute table to obtain value fields associated with their weights and scores as shown in Figure 1. To indicate relative suitability levels of the set of ordered weighting factors, scores ranging from 1 to 3 are given as follows: 1 refers to low suitability, 2 refers to moderate suitability, and 3 refers to high suitability levels. The sum of percentage weight factors equals 100. In case of two overlap datasets, a score of the

Suan Sunandha Science and Technology Journal

features is specified to be 0 based on the overlap criterion when overlapping is not allowed.

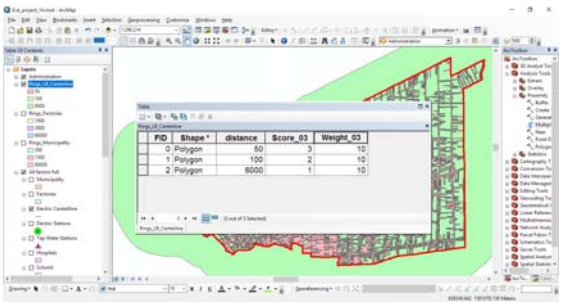

Figure 1. An example of scores and weights given using the Multiple Ring Buffer command with its attribute table

b. Use the Clip function with the output feature of the Multiple Ring Buffer command in order to obtain a dataset coverage equal to the area of the province of Pathumthani as shown in Figure 2.

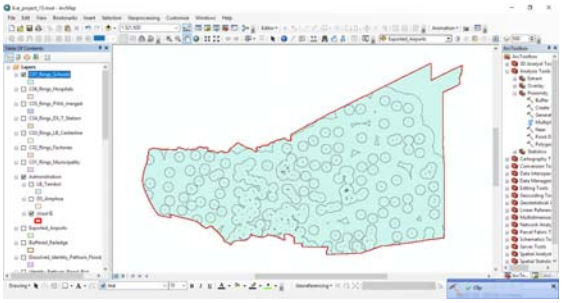

Figure 2. An example of output coverage corresponding to marked geometry of Pathumthani province with the given input dataset

c. Combine multiple datasets of the 12 factors together by using the Union command as shown in Figure 3.

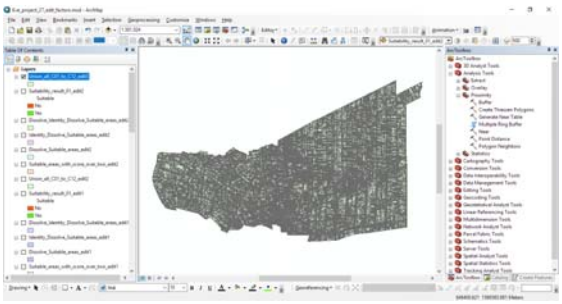

Figure 3. The resulting dataset by combining layers of spatial data and attribute data of all factors

d. Calculate the suitability value of each of resulting feature of the dataset based on the original weights and scores assigned to each factor as shown in Figure 4.

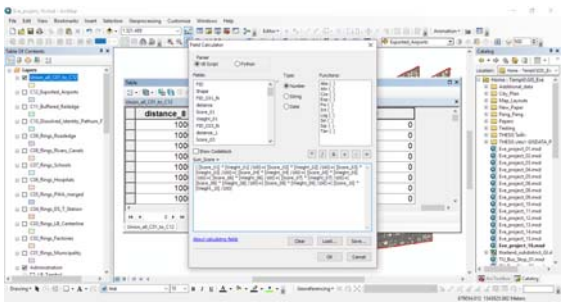

Figure 4. The command and the formula for calculating suitability values of the resulting dataset based on the previously given weights and scores

e. Select features that represent suitable areas for construction of waste-to-energy power plants based on the following criteria: 1) area outside the edge of the province of Pathumthani to avoid the overlapping (areas with original score of 0); and 2) the resulting total score greater than 2.00 indicating the moderately suitable level as shown in Figure 5. Using symbol colors for suitability classification, green is assigned to suitable areas while red is assigned to unsuitable areas as shown in Figure 6.

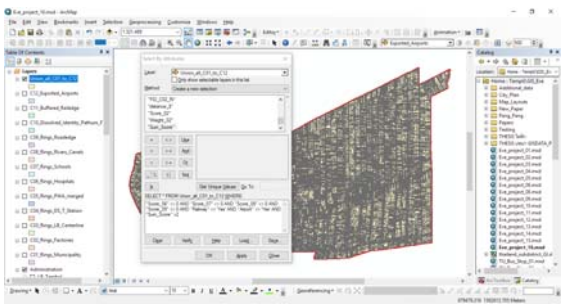

Figure 5. Parameters for selecting suitable areas to build waste-to-energy power plants to meet the criteria for a score of 2.00**.**

Suan Sunandha Science and Technology Journal

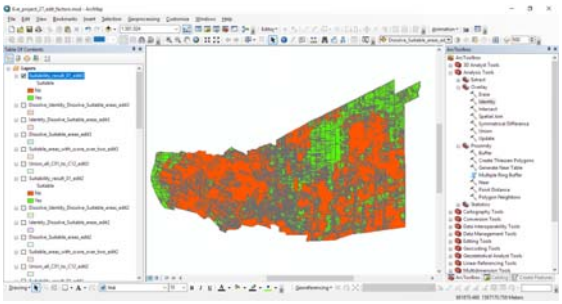

Figure 6. Classification of area suitability for waste-to-energy power plants using symbol colors (green represents suitable areas and red represents unsuitable areas.).

f. Analyze suitable/unsuitable areas of each district in Pathumthani province to generate the output layer by combining the features of the dataset of districts and the output dataset obtained from step (e) using the Identity function.

4. Results

The site suitability assessment areas for waste-to-energy power plants using GIS–OWA technique were used to achieve the suitable/unsuitable area sizes in each district of Pathumthani province as shown in Figure 6 and Tables 2 and 3.

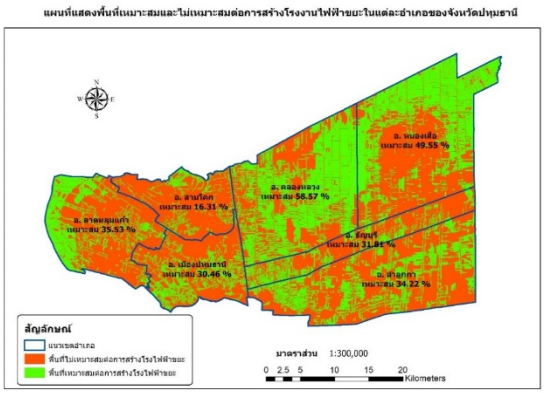

Figure 7. Site suitability analysis for waste-to-energy power plants in each district of Pathumthani province

Table 2. The percentage of suitable/unsuitable areas in Pathumthani province for construction of waste-to-energy power plants

Province/category	Area (rai)	Percent
Pathumthani	950,036.74	100.00
Unsuitable class	562,966.31	59.26
Suitable class	387,070.43	40.74

The analysis result at the provincial level reveals that the total area of Pathumthani of 950,036.74 rai, about 60% is suitable and 40% is unsuitable for construction of waste-to-energy power plant as shown in Table 2.

Table 3. Percentage of suitable/unsuitable areas for construction of waste-to-energy power plants in each district of Pathumthani province with the total area of 950,036.74 rai

District/category		Area (rai)	Percentage of area suitability for each district (%)	Percent area of the province
Pathumthani		**950036.74**		**100.00**
Muang Pathumthani		**89287.55**	**100.00**	**9.40**
	No	62093.81	69.54	6.54
	Yes	27193.74	30.46	2.86
Klong Luang		**189759.28**	**100.00**	**19.97**
	No	78619.27	41.43	8.28
	Yes	111140.00	58.57	11.70
Thanyaburi		**71788.83**	**100.00**	**7.56**
	No	48953.83	68.19	5.15
	Yes	22835.00	31.81	2.40
Ladlumkaew		**122316.25**	**100.00**	**12.87**
	No	78859.89	64.47	8.30
	Yes	43456.36	35.53	4.57
Lamlukka		**190125.99**	**100.00**	**20.01**
	No	125059.40	65.78	13.16
	Yes	65066.59	34.22	6.85
Samkok		**74327.07**	**100.00**	**7.82**
	No	62202.87	83.69	6.55
	Yes	12124.19	16.31	1.28
Nongsua		**212431.77**	**100.00**	**22.36**
	No	107177.23	50.45	11.28
	Yes	105254.54	49.55	11.08

No refers to unsuitable area and Yes refers to suitable area.

As illustrated in Table 3, the suitability rating of the potential areas for construction of waste-to-energy power plants on a scale from high to low is Klong Luang (11.7%), followed by Nongsua (11.08%), Lamlukka (6.85%), Ladlumkaew (4.57%), Muang Pathumthani (2.86%), Thanyaburi (2.4%), and Samkok (1.28%).

Suan Sunandha Science and Technology Journal

5. Conclusion and discussion

The site selection for waste-to-energy power plants in Pathumthani was conducted by the GIS–OWA based suitability analysis with specific range of selection criteria. The result of area suitability analysis revealed that approximately, 60% of total area of Pathumthani was under suitable areas. At the district level, Klong Luang was classified as very highly suitable area, followed by Nongsua. This finding is in agreement with opinions of the inquiring experts and many experienced field operators.

6. Recommendations

The methodology of this study in selecting factors and analyzing the collected data can be further improved and applied to other studied areas by taking into account the physical characteristics of the land and garbage management policy.

7. Acknowledgement

This work would not have been possible without the information provided by Provincial Electricity Authority, Provincial Waterworks Authority and Government office in Pathumthani. The author would like to express our sincere gratitude to the School of Engineering, Thammasat University for the support of the Faculty Research Grants.

8. Conflict of Interest

This research was conducted without any conflicts of interest.

9. References

Ajjima Chansuwanich. (2016), Report of the Integrated Inspection to Drive Important Policy Issues on Waste and Environmental Management in accordance with the Integrated Inspection Plan of the Inspector, the Prime Minister's Office.

Associate Professor Dr.Supetch Jirakajornkun. (2017), learning geographic information system with ArcGIS Desktop 10.5, 1st edition, Nonthaburi, A.P. graphic design and printing

Criteria and Standards for Integrated Town Planning. (2006), *Department of Public Works and Town and Country Planning*, Page 83-86

Electrical power system, searched on 7 December 2019, Retrieved from http://www2.dede.go.th/bhrd/old/Download/file_handbook/Pre_Build/Build_6.pdf

Emergency action plan to solve flood disaster problems Pathum Thani Province. (2014), *Disaster Prevention and Mitigation Office*, Pathum Thani Province

Goyal, H., Sharma, C., & Joshi, N. (2017). An Integrated Approach of GIS and Spatial Data Mining in Big Data. *International Journal of Computer Applications*, 169(11), 1-6.

Hazardous waste, searched on 7 December 2019, Retrieved from http://www.falmouthmass.us/695/Household-Hazardous-Waste-Collection

Krabi Town Planning and Planning Project (2014), Department of Public Works and Town and Country Planning, Page 134-189

Misra, S., & Sharma, S. (2015). Site Suitability Analysis for Urban Development: A Review. *International Journal on Recent and Innovation Trends in Computing and Communication*, 3(6), 3647-3651.

Naphon Surongkharat and Dr. Tulawit Sathonjanu (2013), finding suitable area for biomass power plant from rubber wood in Rayong, *KKU Research Journal (GS)*

Opas Iamsiriwong. (2015), Database System, Bangkok, SE-Education

Piyachart Artuwan. (2 0 1 4) , Academic Article Community waste, the big problem that the country is facing, *the Office of Academic Affairs Secretariat of the Senate*, Year 4, Issue 7, Page 2-8

Power transmission system, searched on October 2, 2019, Retrieved from http://dspace.spu.ac.th/handle/123456789/464

Private electricity supplier, searched on November 3, 2019, Retrieved from http://www.eppo.go.th/index.php/th/electricity/private

Rikalovic, A., Cosic, I., & Lazarevic, D. (2014). GIS Based Multi-Criteria Analysis for Industrial Site Selection. *Procedia Engineering, 69*(2014), 1054–1063. doi: 10.1016/j.proeng.2014.03.090

The concept of waste to energy power plant prototype, searched on November 11, 2019, Retrieved from https://techsauce.co/tech-and-biz/waste-to-energy-ace-electricity

Suan Sunandha Science and Technology Journal

Urban Planning and Planning Project for Pathum Thani Province (2014), Department of Public Works and Town Planning

Zabihi, H., Alizadeh, M., Langat, P., Karami, M., Shahabi, H., Ahmad, A., Said, M., & Lee, S. (2019). GIS Multi-Criteria Analysis by Ordered Weighted Averaging (OWA): Toward an Integrated Citrus Management Strategy. *Sustainability*,*11*(1009),1-17. doi:10.3390/su11041009

Available online at http://www.ssstj.sci.ssru.ac.th

SSSTJ

Suan Sunandha Science and Technology Journal

A Polymeric Coating on Prelithiated Silicon-Based Nanoparticles for High Capacity Anodes used in Li-ion Batteries

Natthaphong Kamma[1], Yutthanakon Kanaphan[1], Sunisa Buakeaw[1], Songyoot Kaewmala[2], Chirapan Chaikawang[2], Jeffrey Nash[3], Sutham Srilomsak[1,2], Nonglak Meethong[1,2*]

[1]Materials Science and Nanotechnology Program, Department of Physics, Faculty of Science, Khon Kaen University, Khon Kaen 40002, Thailand

[2]Institute of Nanomaterials Research and Innovation for Energy (IN-RIE), Research Network of NANOTEC-KKU (RNN), Khon Kaen University, Khon Kaen 40002, Thailand

[3]Graduate School, Udon Thani Rajabhat University, Udon Thani 41000, Thailand

Corresponding author e-mail: *nonmee@kku.ac.th

Received: *5 March 2020* / **Revised**: *13 March 2020* / **Accepted:** *10 April 2020*

Abstract

Silicon is a promising candidate anode material for lithium ion batteries due to its high theoretical specific capacity of 4,200 mAh g^{-1} and low discharge potential. However, a high irreversible capacity loss due to a solid electrolyte interphase formation on the surface of Si anodes during the 1st cycle limits its practical applications. Prelithiation is considered an attractive method that can be used to compensate for the active lithium losses during the 1st cycle. Surface oxidation to Li_2O when the material comes into contact with moisture and oxygen during electrode fabrication is a main obstacle, leading to poor electrochemical stability. In this work the surface stability of prelithiated Si-based nanoparticles was modified via a polymeric nano-coating method. The results demonstrate that coating with 1-fluorooctane is an effective strategy to mitigate irreversible capacity loss and provide electrochemical stability for high performance next generation lithium ion batteries.

Keywords: Lithium ion batteries, Silicon, Prelithiation

1. Introduction

Lithium ion batteries (LIBs) are playing an essential role in the development of electric vehicles (EVs) and grid energy storage technologies owing to their high energy density, low self-discharge, and long cycle life (Kennedy, Patterson, & Camilleri, 2000; Tarascon & Armand, 2001). Silicon (Si) represents an attractive candidate anode material to replace commercial graphite as a way of improving the energy density of LIBs. This is due to its high theoretical specific capacity of 4,200 mAh g^{-1} (through the formation of a $Li_{4.4}Si$ alloy). This is ten times higher than that of commercial graphite anodes with a relatively low electrochemical potential (370 mV) (Kasavajjula, Wang, & Appleby, 2007; Yin, Wan, & Guo, 2012). However, practical applications that achieve a satisfactory high capacity and stable cycling performance have not been realized since a large volume change (>400%), (Hui Wu & Cui, 2012) causes mechanical stress within the electrode leading to its rapid structural failure and poor electrical contact with the active material (Beaulieu, Eberman, Turner, Krause, & Dahn, 2001; Domi, Usui, Iwanari, & Sakaguchi, 2017).

Therefore, novel nanostructural designs of silicon-based electrode materials have been utilized to mitigate the volume expansion of the silicon structure and improve its cycling performance (N. Liu, Li, Pasta, & Cui, 2014; N. Liu et al., 2014; Son et al., 2015; Hui Wu & Cui, 2012). This can be facilitated by effective diffusion of active lithium and electrons (Y. Wang, Li, He, Hosono, & Zhou, 2010). However, a drawback to this approach is that the high surface area of these nanostructured materials significantly increases solid electrolyte interphase (SEI) formation during the first cycle (Aurbach, 1994). SEI formation on silicon anodes during the first cycle causes highly irreversible

Suan Sunandha Science and Technology Journal

capacity losses of 50-80% and can result in low Coulombic efficiency (CE) (DiLeo et al., 2013; Hu et al., 2013; H. Wu et al., 2013; X. Wu, Wang, Chen, & Huang, 2003) depending on the structure of the silicon and the composition of the anode composite. The irreversible loss of active lithium anode material during the first cycle can be mitigated by prelithia-tion, which has been previously achieved. Experi-mentally, the commercial prelithiation reagent used is stabilized lithium metal powder (SLMP). It can be drop-cast onto on an electrode material serving as an anode, such as graphite, SiO_2, Si or CNT-based electrodes (Forney, Ganter, Staub, Ridgley, & Landi, 2013; Z. Wang et al., 2014). However, SLMP is hard to synthesize and is inhomogeneously distri-buted within the electrodes. Another approach is to use mechanical stirring of the Si anode material with Li metal at high temperatures to form Li_xSi NPs (Yom, Seong, Cho, & Yoon, 2018; Zhao et al., 2014; Zhao et al., 2018). The resulting material suffers from surface oxidation that forms a Li_2O passivation layer when in contact with moisture and oxygen converting Li_xSi to $Li_xSi{-}Li_2O$ NPs with a rather low potential and high capacity. These Li_xSi NPs anode materials with fine structures typically show improved electrochemical performance and worsened stability on exposure to air with high relative humidity (RH) (Zhao et al., 2015). Therefore, surface coating may be an appropriate alternative to improve stability and yield higher capacities. For example, Li_xSi NPs mixed with poly(styrene-butadiene-styrene) (SBS) polymer and graphene can be used as an anode (Zhao et al., 2017a). Also, Li_xSi NPs can be protected by an artificial solid electrolyte interphase (Liu et al., 2017; Zhao et al., 2015; Zhao et al., 2017b). These coatings are effective to some extent and it is still necessary use them in a dry room.

This work proposes a polymeric-coating on the surface of prelithiated Si-based NPs (Li_xSi NPs). They are made using a prelithiation method to fabricate electrode materials that compensate for first-cycle capacity losses and reduce the unwanted reactions encountered by Li_xSi NPs exposed to air or other reactive environments. These materials are prepared using a thermal prelithiation forming a polymer shell around the NPs in a reaction of Li_xSi NPs with 1-fluorooctane, thereby producing a continuous and dense coating over the Li_xSi NPs. The 1-fluorooctane was selected because of its excellent chemical behavior in nonpolar solvents such as cyclohexane. It is highly reactive with Li_xSi NPs (Zhao et al., 2014). The LiF and other lithium compounds with long hydrophobic carbon chains effectively protect the reactivity of Li_xSi NPs when exposed to an ambient environment though the formation of a dense outer coating (Zhao et al., 2015). It is of great importance to develop relatively stable coated-Li_xSi NPs, which can be easily handled during the process of battery assembly.

2. Experimental

2.1 Materials preparation

40 and 80 µL aliquots of 1-fluorooctane ($CH_3(CH_2)_7F$, Sigma Aldrich) were each mixed in 20 ml of anhydrous cyclohexane and then stirred at 60 ºC for 2 h. Next, Li_xSi NPs (200 mg) were synthesized via a modified hydride destabilization method (Vajo, Mertens, Ahn, Bowman, & Fultz, 2004). These Li_xSi NPs were dispersed in anhydrous cyclohexane (Sigma Aldrich) with vigorous stirring for 1 h to obtain a suspension with 5 mg ml^{-1} of Li_xSi NPs. The 40 µL 1-fluorooctane solution and the Li_xSi NP suspension were homogeneously mixed at room temperature inside a glovebox under an Ar atmosphere for 1 h with vigorous stirring. After mixing, the coated-Li_xSi NPs were washed with cyclohexane and centrifuged to remove unreacted 1-fluorooctane and then dried under a vacuum. This process was repeated using the 80 µL 1-fluorooctane mixture. The samples made up with 40 and 80 µL aliquots of 1-fluorooctane are referred to as the coated-40 and coated 80 samples, respectively.

2.2 Structural and Morphological characterization

X-ray diffraction (XRD) (PANalytical, Empy-rean) was performed to examine the crystal structure of the experimental samples using Cu-Kα radiation with a step size of 0.01° and over a 2θ range of 10°-80°. Transmission electron microscopy (FEI, TECNAI G220) was used to investigate the microstructural properties of the Li_xSi-coated NP materials.

2.3 Electrochemical testing

Swagelok type cells were assembled in an Ar-filled glove box to evaluate the electrochemical properties of these materials. The Li_xSi or coated-Li_xSi NP materials were mixed with carbon black (Super P, Alfa Aesar) and polyvinylidene fluoride (PVDF-Kynar 2801, Arkema) (65:20:15 by weight)

Suan Sunandha Science and Technology Journal

in a 1,3 dioxolane (DOL, Sigma Aldrich) solvent, which was then mechanically stirred to form a slurry. The resulting slurry was coated on copper foil using a doctor blade and then dried under a vacuum at 80 °C overnight. The Swagelok type cells consisted of discs of the prepared anode and a Li metal foil (Alfa Aesar), used as counter and reference electrodes, respectively. A 1.0 M $LiPF_6$ solution in a 1:1 w/w ratio of ethylene carbonate (EC) and dimethyl carbonate (DMC), 1 vol% of vinylene carbonate and 2 vol% of fluoroethylene carbonate was used as an electrolyte with a Celgard 2400 (MTI) separator. Galvanostatic charge/discharge tests were done between 0.01-1.2 V at a C/20 rate (1C = 4.2 A g^{-1}) using a multi-channel tester (BST8 MA, MTI).

3. Results and discussion

The Li_xSi NPs were synthesized via a modified hydride destabilization method using commercial Si, which exhibits surface oxidation that forms a Li_2O passivation layer when in contact with moisture and oxygen during the synthesis of LixSi NPs. This leads to poor electrochemical stability. Therefore, modifying the surface of Li_xSi NPs was done via a polymeric nano-coating with the reduction of 1-fluorooctane in cyclohexane, as depicted in Figure 1a, to prevent further oxidation. The morphology of the Li_xSi NPs with a size range of 10 to 20 nm and of the coated-40 and coated-80 samples are respectively shown in Figure 1b-d. Generally, the surfaces of Li_xSi NPs consisted of lithium fluoride (LiF) and other lithium compounds such as lithium alkyl carbonates with long hydrophobic carbon chains. This is similar to the reaction mechanism employing butyllithium (Wilke, 2003; Zhao et al., 2015). Li_xSi NPs transfer a single electron to a C−F bond in 1 fluorooctane forming a C radical and F^-, and a second electron transfer converts the C radical into a carbanion (reaction 1). Additionally, O_2 and CO_2 in the glovebox may react with alkyl lithium to form a complex mixture of lithium compounds (reaction 2).

$$F\text{-}(CH_2)_7CH_3 \xrightarrow{Li_xSi} LiF + Li\text{-}(CH_2)_7CH_3 \quad (1)$$

$$Li\text{-}(CH_2)_7CH_3 \xrightarrow{O_2/CO_2} Li\text{-}OC(=O)O\text{-}(CH_2)_7CH_3 \quad (2)$$

The XRD patterns of all the uncoated and coated samples are shown in Figure 2. The coated and uncoated samples at 0 h of exposure to ambient air exhibited quite similar XRD patterns, showing diffraction peaks of the $Li_{22}Si_5$ (PDF No. 01-073-2049), $Li_{12}Si_7$ (PDF No. 00-040-0942), Li_2O (PDF No. 01-073-0593), and LiOH phases (space group P4/nmm with PDF No. 01-076-0911, and P4/mmm

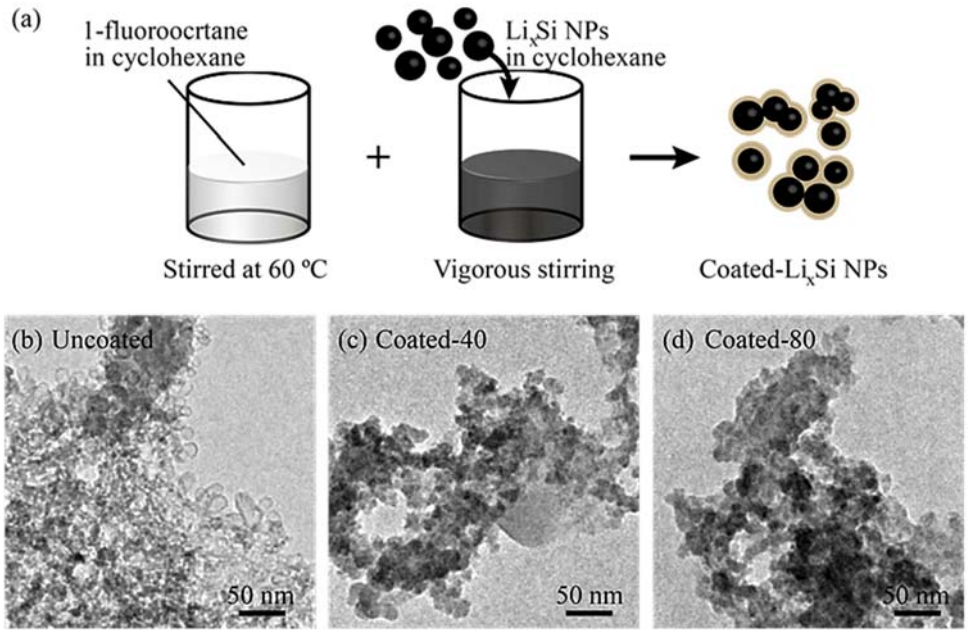

Figure 1. (a) Schematic diagram of the coated Li_xSi NPs passivation layer formed by chemical reactions via 1-fluorooctane. (b-d) TEM images of the Li_xSi NPs, coated-40 and coated-80 samples, respectively.

Suan Sunandha Science and Technology Journal

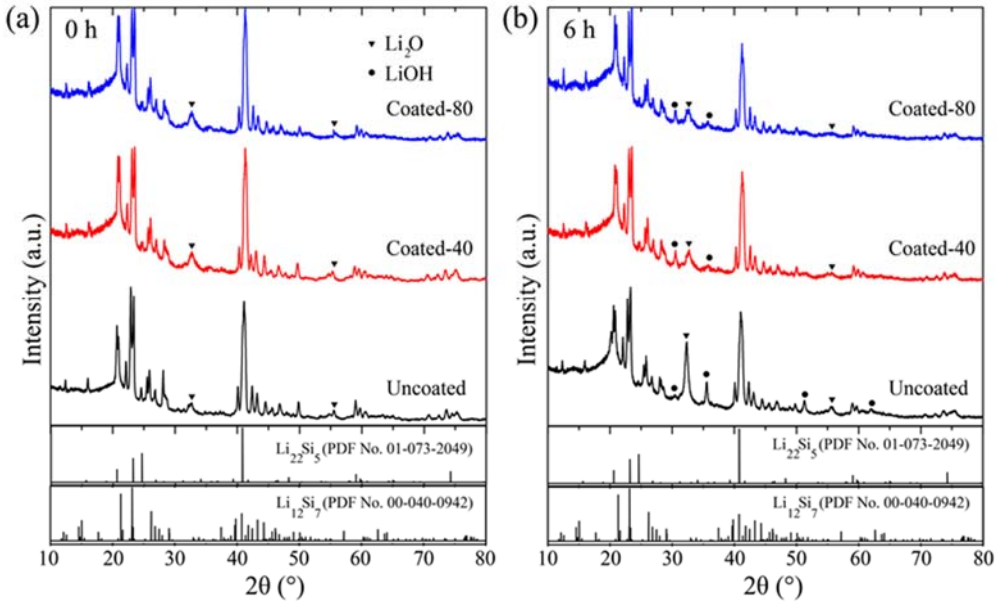

Figure 2. XRD patterns of the uncoated, coated-40 and coated-80 samples after (a) 0 h and (b) 6 h of exposure to ambient air with 20±2% RH.

with PDF No. 00-001-1021) as given in Figure 2a. The $Li_{22}Si_5$ and $Li_{12}Si_7$ phases are formed as a result of the pre-lithiation process, while the Li_2O and LiOH phases are formed due to reactions with O_2 and water vapor in the ambient environment. The coated and uncoated samples at 6 h of exposure to ambient air with 20±2% RH showed different amounts of Li_2O and LiOH phases compared to those with 0 h of exposure. After exposure to ambient air for 6 h, the XRD pattern of the uncoated sample showed significantly higher peak intensities of the Li_2O and LiOH phases. However, the XRD patterns of the coated samples showed similar peak intensities of these phases. The coated-80 sample showed slightly lower amounts of Li_2O and LiOH phases than that of the coated-40 sample due to a thicker surface coating. This indicates that our method using polymeric coating can effectively protect pre-lithiated Li_xSi NPs and prevent further surface oxidation for at least 6 h. This polymeric coating method is effective because both LiF and lithium alkyl carbonate with long hydrophobic carbon chains can serve to form an effective passivation layer on the surfaces of Li_xSi NPs, retarding reactions of metallic lithium with O_2 and water vapor in an ambient environment (Stubblefield & Bach, 1972; Zhao et al., 2017b).

A study of the electrochemical properties of the initial Li_xSi NPs and coated-Li_xSi NP materials (coated-40 and coated-80 sample) at 20±2% RH after 0 h, 6 h, and 24 h exposure to ambient air was carried out using Swagelok type cells. All samples were fabricated using Li metal as counter electrodes. The electrolyte solution consisted of 1.0 M $LiPF_6$ in a 1:1 w/w ratio of ethylene carbonate (EC) and dimethyl carbonate (DMC), 1 vol% of vinylene carbonate and 2 vol% of fluoroethylene carbonate with a Celgard 2400 disc as a separator. All the specific capacities and current densities are reported based on the weight of active material in the anodes. The electrochemical behaviour of the initial Li_xSi NPs and coated-Li_xSi NP anodes was evaluated using galvanostatic charge/discharge measurements during their first cycle (Figure 3a-c). The samples after 0 h of exposure showed first charge capacities of about 1,395, 1,371 and 1,091 mAh g^{-1} for the uncoated, coated-40 and coated-80 samples, respectively. After exposure to an ambient environment with 20±2% RH for 6 h, the uncoated sample showed negligible capacity, while the coated-40 sample retained 839 mAh g^{-1} and the coated-80 sample retained 1,025 mAh g^{-1}. This indicates that the coated-40 sample showed a capacity decay of 39% while the coated-80 sample lost less than 6% of its capacity. After 24 h of exposure to the ambient environment, the coated 40 sample exhibited a capacity of 405 mAh g^{-1}, which is a capacity decay of 70% of its initial capacity. The coated-80 sample still delivered a stored capacity of 677 mAh g^{-1}, which is a capacity decay of 38% of its

Suan Sunandha Science and Technology Journal

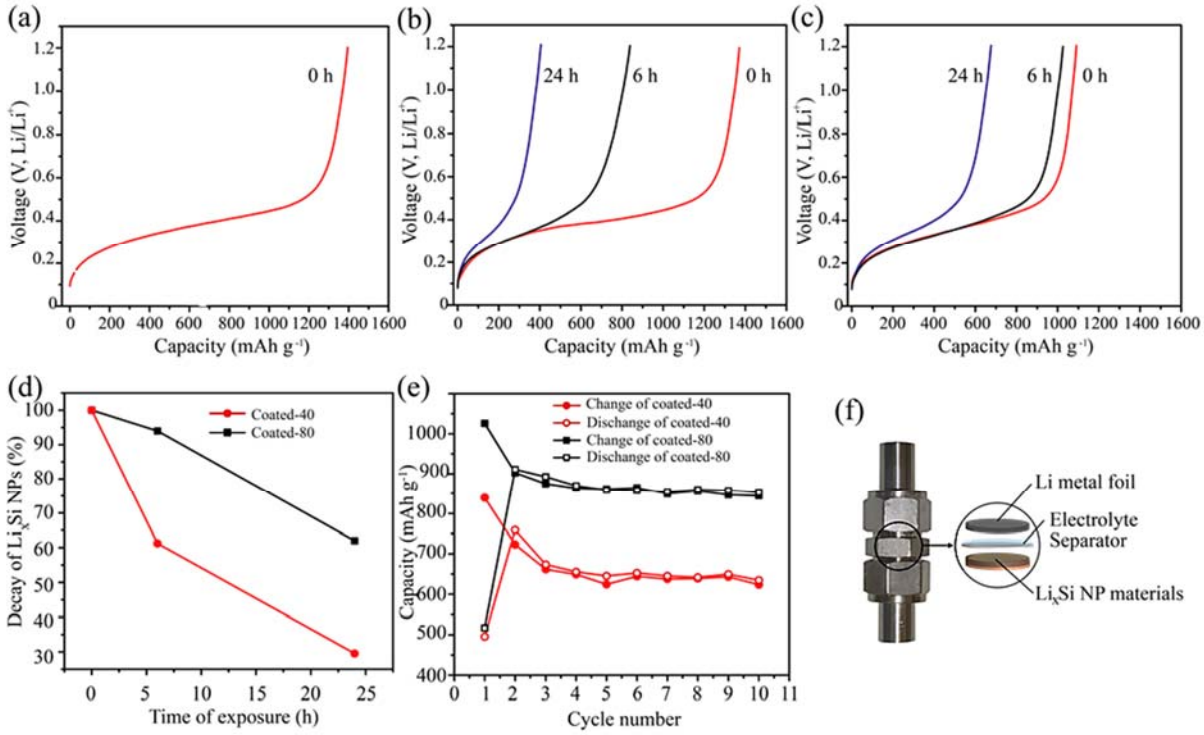

Figure 3. Voltage profiles during first charging cycle of (a) uncoated (b) coated-40 (c) coated-80 samples under ambient conditions for various durations (20±2% RH) (d) the change in capacity of the coated anodes as a function of exposure time, (e) the cycling stability of the electrodes prepared from the 6 h air exposed coated-40 and coated-80 samples at a C/20 rate (1C = 4.2 A g^{-1}) (f) the Swagelok type cell for electrochemical testing.

initial capacity. This indicates that even though the coated-80 sample was protected from further surface oxidation for about 6 h, the coating thickness needs to be optimized to prevent reactions of metallic lithium with O_2 and water vapor in an ambient environment for longer exposure times. This topic will be our focus in future experiments. Figure 3d summarizes the results of effect of air exposure.

Figure 3e shows the cycling performance of the electrodes prepared from the coated-40 and coated-80 samples after 6 h of exposure to ambient air. It is noteworthy that the cycling stability of the 6 h air exposed coated-40 sample was quite similar to that of the coated-80 sample. However, the absolute discharge capacity after 6 h at 20±2% RH of the coated-80 sample was higher than that of the coated-40 sample. The discharge capacities after 10 cycles were ~860 and ~630 mAh g^{-1} for the coated-80 and coated-40 samples, respectively. This shows that the discharge capacity of the coated samples was a function of the concentration of the 1-fluorooctane used in forming the coating. A thicker coating is more effective in preventing reactions with O_2 and moisture resulting in superior electrochemical performance.

4. Conclusions

We successfully developed a polymeric coating method for pre-lithiated Li_xSi NPs, with a size range of 10-20 nm, using a chemical reaction involving 1-fluorooctane. LiF and lithium alkyl carbonate compounds with long hydrophobic carbon chains can serve as an effective passivation layer on the surfaces of Li_xSi NPs. This polymeric coating layer can retard reactions of metallic lithium with O_2 and water vapor inhibited negative reactions under ambient conditions, improved electrochemical performance, and improved the ease of electrode fabrication. The coated-40 and coated-80 samples showed similar capacity decays in an ambient environment at 20±2% RH after 6 h, but the coated-80 sample had higher capacities after 10 cycles. This indicates that polymer coating methods are potentially useful in industrial battery fabrication. Thus, application of polymeric coatings on the surfaces of lithium containing anode materials is a promising approach that may facilitate prelithiation

Suan Sunandha Science and Technology Journal

methods for high performance next generation lithium ion batteries.

Acknowledgement

This work has been partially supported by the Institute of Nanomaterials Research and Innovation for Energy (IN-RIE), Khon Kaen University. N. M. acknowledges partial support by Research Network NANOTEC (RNN), NSTDA, Ministry of Higher Education, Science, Research and Innovation and Khon Kaen University, Thailand.

References

Aurbach, D. (1994). The correlation between the surface chemistry and the performance of Li-carbon intercalation anodes for rechargeable 'Rocking-Chair' type batteries. Journal of The Electrochemical Society, 141(3), 603. doi: 10.1149/1.2054777

Beaulieu, L., Eberman, K., Turner, R., Krause, L., & Dahn, J. (2001). Colossal reversible volume changes in lithium alloys. Electrochemical and Solid-State Letters, 4(9), A137-A140. doi: 10.1149/1.1388178

DiLeo, R. A., Ganter, M. J., Thone, M. N., Forney, M. W., Staub, J. W., Rogers, R. E., et al. (2013). Balanced approach to safety of high capacity silicon–germanium–carbon nanotube free-standing lithium ion battery anodes. Nano Energy, 2(2), 268-275. doi: 10.1016/j.nanoen.2012.09.007

Domi, Y., Usui, H., Iwanari, D., & Sakaguchi, H. (2017). Effect of mechanical pre-lithiation on electrochemical performance of silicon negative electrode for lithium-ion batteries. Journal of The Electrochemical Society, 164(7), A1651-A1654. doi: 10.1149/2.1361707jes

Forney, M. W., Ganter, M. J., Staub, J. W., Ridgley, R. D., & Landi, B. J. (2013). Prelithiation of silicon-carbon nanotube anodes for lithium ion batteries by stabilized lithium metal powder (SLMP). Nano letters, 13(9), 4158-4163. doi: 10.1021/nl401776d

Hu, L., Liu, N., Eskilsson, M., Zheng, G., McDonough, J., Wågberg, L., et al. (2013). Silicon-conductive nanopaper for Li-ion batteries. Nano Energy, 2(1), 138-145. doi: 10.1016/j.nanoen.2012.08.008

Kasavajjula, U., Wang, C., & Appleby, A. J. (2007). Nano- and bulk-silicon-based insertion anodes for lithium-ion secondary cells. Journal of Power Sources, 163(2), 1003-1039. doi: 10.1016/j.jpowsour.2006.09.084

Kennedy, B., Patterson, D., & Camilleri, S. (2000). Use of lithium-ion batteries in electric vehicles. Journal of Power Sources, 90(2), 156-162. doi: 10.1016/S0378-7753(00)00402-X

Liu, N., Li, W., Pasta, M., & Cui, Y. (2014). Nanomaterials for electrochemical energy storage. Frontiers of Physics, 9(3), 323-350. doi: 10.1007/s11467-013-0408-7

Liu, N., Lu, Z., Zhao, J., McDowell, M. T., Lee, H. W., Zhao, W., et al. (2014). A pomegranate-inspired nanoscale design for large-volume-change lithium battery anodes. Nature Nanotechnology, 9(3), 187-192. doi: 10.1038/nnano.2014.6

Liu, Y., Lin, D., Yuen, P. Y., Liu, K., Xie, J., Dauskardt, R. H., et al. (2017). An artificial solid electrolyte interphase with high Li-ion conductivity, mechanical strength, and flexibility for stable lithium metal anodes. Advanced Materials, 29(10). doi: 10.1002/adma.201605531

Son, I. H., Hwan Park, J., Kwon, S., Park, S., Rummeli, M. H., Bachmatiuk, A., et al. (2015). Silicon carbide-free graphene growth on silicon for lithium-ion battery with high volumetric energy density. Nature Communications, 6, 7393. doi: 10.1038/ncomms8393

Stubblefield, C. B., & Bach, R. O. (1972). Solubility of lithium fluoride in water. Journal of Chemical and Engineering Data, 17(4), 491-492. doi: 10.1021/je60055a017

Tarascon, J. M., & Armand, M. (2001). Issues and challenges facing rechargeable lithium batteries. Nature, 414, 359-367. doi: 10.1038/35104644

Vajo, J. J., Mertens, F., Ahn, C. C., Bowman, R. C., & Fultz, B. (2004). Altering hydrogen storage properties by hydride destabilization through alloy formation: LiH and MgH_2 destabilized with Si. The Journal of Physical Chemistry B, 108(37), 13977-13983. doi: 10.1021/jp040060

Wang, Y., Li, H., He, P., Hosono, E., & Zhou, H. (2010). Nano active materials for lithium-ion batteries. Nanoscale, 2(8), 1294-1305. doi: 10.1039/C0NR00068J

Suan Sunandha Science and Technology Journal

Wang, Z., Fu, Y., Zhang, Z., Yuan, S., Amine, K., Battaglia, V., et al. (2014). Application of stabilized lithium metal powder (SLMP®) in graphite anode - A high efficient prelithiation method for lithium-ion batteries. Journal of Power Sources, 260, 57-61. doi: 10.1016/j.jpowsour.2014.02.112

Wilke, G. (2003). Fifty years of Ziegler catalysts: consequences and development of an invention. Angewandte Chemie International Edition, 42(41), 5000-5008. doi: 10.1002/anie.200330056

Wu, H., & Cui, Y. (2012). Designing nanostructured Si anodes for high energy lithium ion batteries. Nano Today, 7(5), 414-429. doi: 10.1016/j.nantod.2012.08.004

Wu, H., Yu, G., Pan, L., Liu, N., McDowell, M. T., Bao, Z., et al. (2013). Stable Li-ion battery anodes by in-situ polymerization of conducting hydrogel to conformally coat silicon nanoparticles. Nature Communications, 4, 1943. doi: 10.1038/ncomms2941

Wu, X., Wang, Z., Chen, L., & Huang, X. (2003). Ag-enhanced SEI formation on Si particles for lithium batteries. Electrochemistry Communications, 5(11), 935-939. doi: 10.1016/j.elecom.2003.09.001

Yin, Y., Wan, L., & Guo, Y. (2012). Silicon-based nanomaterials for lithium-ion batteries. Chinese science bulletin, 57(32), 4104-4110. doi: 10.1007/s11434-012-5017-2

Yom, J. H., Seong, I. W., Cho, S. M., & Yoon, W. Y. (2018). Optimization of heat treatment conditions for fabricating pre-lithiated silicon monoxide as an anode material for lithium-ion batteries. Journal of The Electrochemical Society, 165(3), A603-A608. doi: 10.1149/2.0911803jes

Zhao, J., Lu, Z., Liu, N., Lee, H. W., McDowell, M. T., & Cui, Y. (2014). Dry-air-stable lithium silicide-lithium oxide core-shell nanoparticles as high-capacity prelithiation reagents. Nature Communications, 5, 5088. doi: 10.1038/ncomms6088

Zhao, J., Lu, Z., Wang, H., Liu, W., Lee, H. W., Yan, K., et al. (2015). Artificial solid electrolyte interphase-protected Li_xSi nanoparticles: an efficient and stable prelithiation reagent for lithium-ion batteries. Journal of the American Chemical Society, 137(26), 8372-8375. doi: 10.1021/jacs.5b04526

Zhao, J., Zhou, G., Yan, K., Xie, J., Li, Y., Liao, L., et al. (2017a). Air-stable and freestanding lithium alloy/graphene foil as an alternative to lithium metal anodes. Nature Nanotechnology, 12(10), 993-999. doi: 10.1038/nnano.2017.129

Zhao, J., Liao, L., Shi, F., Lei, T., Chen, G., Pei, A., et al. (2017b). Surface fluorination of reactive battery anode materials for enhanced stability. Journal of the American Chemical Society, 139(33), 11550-11558. doi: 10.1021/jacs.7b05251

Zhao, J., Sun, J., Pei, A., Zhou, G., Yan, K., Liu, Y., et al. (2018). A general prelithiation approach for group IV elements and corresponding oxides. Energy Storage Materials, 10, 275-281. doi: 10.1016/j.ensm.2017.06.013

Available online at http://www.ssstj.sci.ssru.ac.th

SSSTJ

Suan Sunandha Science and Technology Journal

Acute and Chronic Toxicity of Battery Waste Leachates to *Daphnia magna*

Van-Tai Nguyen[1], The-Ton Phan[1], Thi-My-Chi Vo[1], Thanh-Luu Pham[2], Manh-Ha Bui[3], Thanh-Son Dao[1*]

[1]Ho Chi Minh City University of Technology, VNU-HCM, Vietnam
[2]Institute of Tropical Biology, Vietnam Academy of Science and Technology, Vietnam
[3]Department of Environmental Sciences, Saigon University, Vietnam
Corresponding author e-mail: [*]dao.son@hcmut.edu.vn

Received: *4 April 2020* / **Revised:** *20 April 2020* / **Accepted:** *24 April 2020*

Abstract

In developing countries, e-waste battery treatment and management is a severe problem. Most batteries contain heavy metals, but some can contain very toxic heavy metals such as mercury that can be hazardous to the environment. The current investigation aims to evaluate both the acute and chronic effects of the leachates from two cells (named Con O and Maxell) that are commonly used in Vietnam on the micro-crustacean *Daphnia magna*. The median lethal concentrations at 24h and 48h (LC_{50}) of the *D. magna* exposed to leachate from Con O cell were 150 and 100 mg/l, respectively. The 24h- and 48h-LC_{50} values of the Maxell cell to the animals were 100 and 70 mg/l, respectively. Therefore, the toxicity of the leachates from the Maxell battery was more severe than that of Con O based on the 24h- and 48h-LC_{50} values. Moreover, the life-history traits of the *D. magna* such as survivorship, maturation or reproduction, were detrimentally impacted including mass mortality, delayed maturation and reproductive inhibition, when the animals exposed to the leachates from both batteries at the concentrations ranged from 1 to 50 mg/l over the period of 2 weeks. Overall, this study could provide useful information on the ecological and environmental risk caused by untreated batteries to the environment, or even contribute to changing a sense of civic responsibility on economically using, recycling, waste management and treatment related to cells.

Keywords: Negative effects, Battery leachates, Life history traits, *Daphnia magna*

1. Introduction

Due to the development in the energy industry, the vast battery consumption (e.g., in portable electrical or electronic devices) along with short life span has resulted in the generation of a large number of spent batteries (Meshram, Abhilash, Pandey, Mankhand, & Deveci, 2016). For instance, according to the report on hazardous household waste generation in Japan (Yasuda & Tanaka, 2006), used batteries constituted about 52-71% of the household hazardous waste. Besides, their recovery is also tricky and not economically feasible as they are used in alloys with other metals such as iron or in low concentration (Peiro, Mendez, & Ayres, 2013). In developing countries, such as Vietnam, the used batteries are not well managed and treated. The e-waste batteries (e.g. in houses, offices, entertainment services, etc.) are put into the trash then end in a landfill. This would be a sink and source of pollutants leached out of the e-waste batteries to the environment. Seriously, almost batteries contain several materials (e.g., trace metal, plastics, see Table 1) that can be extremely harmful to human health and ecosystems if they are not treated suitably. Hence, the untreated or not adequately treated wastewater from the landfill would contain leachates from batteries and enter natural water of lakes, ponds, reservoirs, rivers. Theoretically, in water bodies, the pollutant-containing leachates at certain concentrations would impact living things in ecosystems such as zooplankton among others (e.g. phytoplankton, fish, mollusks, amphibians, mammals, aquatic macrophytes).

In the aquatic ecosystem, micro-crustaceans (e.g., *Daphnia magna*) play an essential role in the matter and energy fluxes (Sterner, 2009). Hence they are among the most vulnerable organisms to toxic chemicals in water bodies. Recently, there have been numerous investigations on the single

Suan Sunandha Science and Technology Journal

effects on animals of significant components in batteries including trace metals (e.g., Pb, Zn) and plasticizers (e.g., Tris (2-butoxyethyl) phosphate, polyethylene terephthalate) (Araujo, Pavlaki, Soares, Abessa, & Loureiro, 2019; Giraudo et al., 2017; Luciana, Ulises, Susana, Horacio, & Maria, 2014; Wagner & Oehlmann, 2009). However, there is gap information on the detrimental impacts of untreated batteries on aquatic animals, especially zooplankton. Hence this study aims to evaluate the effects of spent batteries on the life-history traits of *Daphnia magna*.

Table 1. Zinc carbon battery composition (Fisher, Wallén, Laenen, & Collins, 2006).

Components	Percentage (%)
Iron & Steel	16.8
Manganese	15.0
Lead	0.1
Zinc	19.4
Other metals	0.8
Alkali	6.0
Carbon	9.2
Paper	0.7
Plastics	4.0
Water	12.3
Other nonmetals	15.2

2. Materials and Methods

2.1 Materials

In this experiment, two leachates from the used batteries (named Con O and Maxell batteries) were prepared. In Vietnam, these two batteries are common products and widely used in houses, offices as energy supplies for clockwatch, children toys, electric remote device controllers, cassette recorder, and services and entertainments. However, these batteries are not rechargeable and got unique collected, recycled and treated in Vietnam. Consequently, the used batteries have been mainly emitted into the environment as solid waste and ended up in landfills.

The preparing process for the battery leachates was similar to the natural digestion of those in the aquatic environment. Briefly, before the test, five cells of each type (either Con O or Maxell batteries) were weighed and separately placed in the 1-litre plastic bottle containing 250 ml of distilled water. The average weight of one Con O and one Maxell batteries was 14.21 g and 17.35 g, respectively. Afterwards, these bottles were placed outdoor under the sunlight over a period of 14 days. Therefore, the mother solutions of leachates from Con O and Maxell were around 280,000 mg/l and 340,000 mg/l, respectively. Finally, the leachates from the two kinds of electrochemical cells or mother solutions were utilized to test the toxicity to the micro-crustacean (*D. magna*).

Daphnia magna was obtained from Micro Biotest Company (Belgium) and has been maintained in the ISO medium for many generations under the laboratory conditions at the temperature of 25±1°C, the light intensity of 1,000 Lux, and photoperiod of 14 h light: 10 h dark (American Public Health Association [APHA], 2012). Besides, *D. magna* was fed with a mixture of green alga (*Chlorella* sp.) and YTC (yeast, cerrophyl and trout chow digestion) (U.S. Environmental Protection Agency [U.S. EPA], 2002).

2.2 Experimental setup

2.2.1 Acute toxicity of electrochemical cell leachates to *Daphnia magna*

Acute experiments were conducted following the guideline of APHA (2012) and the U.S. EPA (2002) with minor modifications. Firstly, fifty healthy adult female *D. magna* were randomly chosen and cultured in the 1-litre glass beaker containing 800 ml ISO medium. After one night, neonates (less than 24 h old) were randomly collected to prepare for acute experiments. The *D. magna* neonates were fed *ad libitum* with food (*Chlorella* sp. and YTC) two hours before the test. The experiment was implemented at 8 different concentrations including 0 (control), 50, 75, 100, 150, 200, 250 and 300 mg/l of each electrochemical cell leachates.

The pH values in each treatment including the control at the beginning and end of the test were measured, ranged from 6.3-7.3, that was similar with the requirement of APHA (2012) for the acute toxicity test. For each concentration, ten neonates were incubated in a 50 ml glass beaker containing 40 ml of ISO medium. There were four replicates (n = 4) in each treatment, and the test organisms

Suan Sunandha Science and Technology Journal

were not fed during 48 h of the acute experiment. The survival of the test organisms was recorded after 24 h and 48 h of incubation. Dead organisms (defined as the heartbeat stop observed under a microscope) were counted and discarded. The survivorship of test organisms was recorded to determine the concentration of these leachates that killed 50% of the total test animals for 24 h and 48 h (24h- and 48h-LC_{50} values, respectively).

2.2.2 Chronic toxicity of electrochemical cell to *Daphnia magna*

Chronic experiments to evaluate the toxicity of leachates from batteries Con O and Maxell were conducted according to APHA (2012) and Adema (1978). The offspring (less than 24 h old) were also randomly collected and exposed to the leachate from Con O or Maxell battery at four distinct concentrations of 0 (control), 1, 5, and 50 mg/l. For each test concentration, we prepared at once 4 litres of a medium, ISO only (for the control) and ISO containing leachates (at 1, 5 and 50 mg/l of each battery, for exposures). The volume of 4 litres of the medium would be enough for one leachate-concentration test for 14 days of incubation, and to make sure that the leachate concentrations in each test would be constant.

The pH in each test solution remained between 6.2 and 7.3, which also fulfilled conditions for the validity of the chronic toxicity assessment (APHA, 2012). For each concentration, two neonates were incubated together in the 50 ml glass beaker containing 40 ml ISO medium under laboratory conditions as mentioned above, and there were ten replicates (n = 10) in each treatment. While the food (a mixture of *Chlorella* sp. and YTC) was added daily, the medium was totally renewed three times per week during 14 experimental days. The life-history traits of *D. magna,* including survivorship, maturation and reproductive performance, were carefully monitored and recorded daily.

2.3 Data treatment

By the end of the acute test, the Probit analysis program was applied to calculate the 24h- and 48h-LC_{50}. Besides, Kruskal-Wallis test (Sigma Plot 12.0 version) was applied for calculating the statistically significant difference of the maturation of *D. magna* between the control and exposures.

3. Results and Discussion

3.1 Acute toxicity of electrochemical cell leachates to *Daphnia magna*

By the end of the acute tests, 95% of total daphnids in control were still alive well, which was within the requirement of APHA (2012). Nonetheless, the survival proportion of organisms was decreased when exposing to the leachates of both batteries at the concentrations ranged from 50 to 300 mg/l. Particularly, regarding the exposure to the leachate of Con O on *D. magna*, 24h-LC_{50} and 48h-LC_{50} values were 150 (± 20) mg/l and 100 (± 15) mg/l, respectively. Compared to Con O battery, these parameters tested the leachate of Maxell battery were lower, 100 (± 17) mg/l and 70 (± 30) mg/l, respectively (Table 2). That means the toxicity of the leachate from Maxell battery could be more severe than that from Con O to *D. magna*.

Table 2. The 24h- and 48h- lethal concentration of *Daphnia magna* exposed to electrochemical cell leachates of Con O and Maxell.

Leachates from	24h-LC_{50} (mg/l)	48h-LC_{50} (mg/l)
Con O battery	150 ± 20	100 ± 15
Maxell battery	100 ± 17	70 ± 30

Additionally, acute toxicity values on *D. magna* tested with electrochemical cell leachates in the current study seemed to be lower than those of single metals used in the production of batteries (see Table 3). That could be explained by (i) using metallic compound at low concentration in the battery production (Peiro et al., 2013), (ii) the leaching efficiencies of metals used in manufacturing battery (Aaltonen, Peng, Wilson, & Lundstrom, 2017), and (iii) antagonistic interactions between metals due to a competition effect of one metal on the biotic ligand of another metal (Jho, An, & Nam, 2011; Versieren, Smets, De Schamphelaere, Blust, & Smolders, 2014). Moreover, in this study, we did not know exactly toxicants and their concentration in the two battery leachates. Hence, in order to gain insights into the toxicity of the leachates from the electrochemical cell, further chemical analyses (on chemical composition) are suggested.

Table 3. The 48h-LC_{50} values of *Daphnia magna* exposed to metals from previous studies.

Metals	48h-LC_{50} (mg/l)	References
Zn	819 - 928	Shaw, Dempsey, Chen, Hamilton, and Folt (2006); Traudt, Ranville, Smith, and Meyer (2016)
Pb	150 - 450	Biesinger and Christensen (1972); LeBlanc (1982)

Suan Sunandha Science and Technology Journal

Mn	9,300 - 10,270	Biesinger and Christensen (1972); Rathore (2001); Okamoto, Yamamuro, and Tatarazako (2015)
Fe	2,920 - 2,300	Rathore (2001); Okamoto, Yamamuro, and Tatarazako (2015)

3.2 Chronic toxicity of electrochemical cell leachates to *Daphnia magna*

3.2.1 Survivorship of *Daphnia magna*

After two weeks, 85% of total daphnids in the control still actively lived, whereas none of the organisms cultured in the medium containing both leachates at the two high concentrations (5 and 50 mg/l) could be alive. Regarding the lowest concentration (1 mg/l), exposure to the leachates from Con O and Maxell electrochemical cells caused the decrease in the survival proportion of animals, by 20% and 40 %, respectively (Figure 1). It is hypothesized that the metals in the electrochemical cells negatively affected the adsorption capacity and the metabolisms leading to the death of test animals. Similarly, Muyssen, De Schamphelaere, and Janssen (2006) also formulated the hypothesis that chronic exposure to Zn inhibited Ca uptake, resulting in *D. magna* dead as a result of hypocalcemia. Beside Zn, leachates from batteries could contain other trace metals such as Fe, Mn, Pb contributing to the change the concentration of chemicals in organisms suddenly. Almost metals have a high affinity for protein binding sites resulting in their increased toxicity when they occur at relatively high concentrations in the environment (Barata, Baird, Nogueira, Soares, & Riva, 2006). There has been numerous evidence for the synergistic effects upon simultaneous exposure to multiple trace metals on an organism, especially Fe, Mn, Pb and Zn, which are commonly main compositions in batteries (Chu & Chow, 2002; Frías-Espericueta et al., 2008; Kim et al., 2009).

3.2.2 Maturation of *Daphnia magna*

As the batteries contain dozens of harmful chemicals, especially the metal components (see Table 1), not only the survivorship but also the maturation of the organisms could be influenced upon exposure to the electrochemical cell leachates. In the control, the test organisms took around five days to reach maturity. However, there was a statistically significant difference on the maturity age between the control and the exposures at the concentrations from 1 to 5 mg/l in which the exposed animals delayed their maturation, later than 5.5 days. Seriously, the organisms in the exposures at the highest concentrations (50 mg/l) could not mature, although they still lived to the ninth-day of the experiment (Figure 2). That was in line with the result of Ramirez (2014) in which the number of days needed for releasing the first brood increased by one day for metal (Zn, and mixture of Zn and Cd) acclimated animals compared to those in the control. Additionally, trace metals (e.g., Cu, Cr) were demonstrated to cause a delay in the maturation of *D. magna* (Ghazy & Habashy, 2003; Luciana et al., 2014; Nguyen, Vo, Dao, Quang, & Dao, 2016; Tran, Do-Hong, & Dao, 2014).

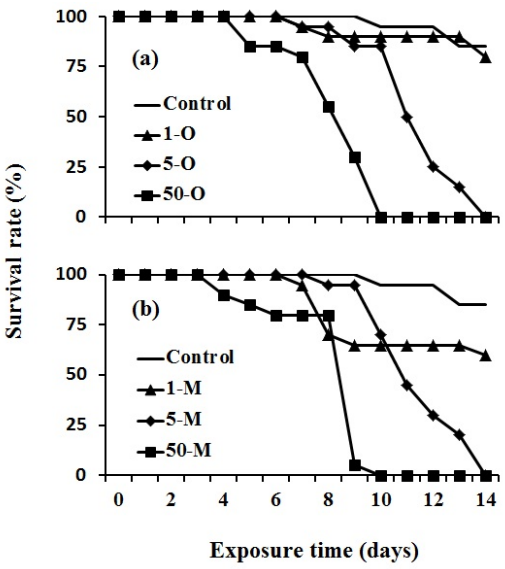

Figure 1. The survival rate of *Daphnia magna* exposed to electrochemical cell leachates of Con O (a), and Maxell batteries (b). 1-O, 5-O, and 50-O, medium containing leachate of 1, 5 and 50 mg/l, respectively, from Con O battery. 1-M, 5-M, and 50-M, medium containing leachate of 1, 5 and 50 mg/l, respectively, from Maxell battery.

Suan Sunandha Science and Technology Journal

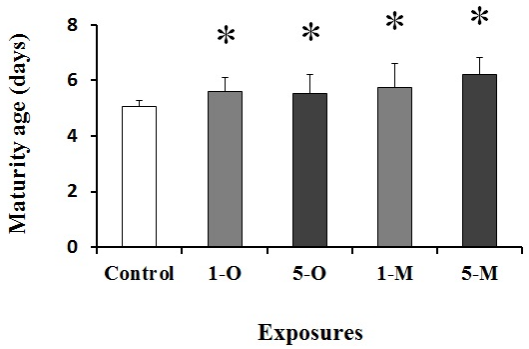

Figure 2. Maturation of *Daphnia magna* exposed to electrochemical cell leachates. The asterisk indicated the significant difference between control and exposures ($p < 0.01$, Kruskal-Wallis test). Abbreviations as in Figure 1.

3.2.3 Reproduction of *Daphnia magna*

According to Kooijman (2000), exposure to trace metals adversely affected the conversion of energy reserves and resources into the number of offspring, which was in agreement with the result in the current study. Additionally, delay in the maturation, as mentioned above, might be one of the main reasons for the reduction in the reproductive performance of *D. magna*. In particular, the total offsprings of *D. magna* in the control was 405 offsprings, whereas compared to the control, those in the exposures to both types of batteries at the lowest concentration (1 mg/l) decreased by more than 40%. Moreover, the reproductive performance of animals in the exposures to the leachates of Con O and Maxell at a concentration of 5 mg/l also reduced sharply by 68% and 74%, respectively. Regarding the organisms exposed to both leachates at the highest concentration (50 mg/l), they did not have any descendants (Table 4).

Table 4. Reproduction of *Daphnia magna* exposed to electrochemical cell leachates of Con O and Maxell.

	Control	Con O cell (mg/l)			Maxell cell (mg/l)		
		1	5	50	1	5	50
Total neonates	405	209	129	0	235	105	0
Proportion to control (%)	100	52	32	0	58	26	0

4. Conclusions

To our best knowledge, there have been few investigations on the impacts of the leachates from used batteries on the organisms. In terms of acute exposure, the leachate from the Maxell battery seems to have higher toxicity to *D. magna* than the other (Con O). The 24h and 48h (LC_{50}) values of the *D. magna* exposed to leachate from Con O cell were 150 and 100 mg/l, respectively. And, the 24h- and 48h-LC_{50} values of the Maxell cell to the animals were 100 and 70 mg/l, respectively. The adversely chronic effects of the leachate from two commonly used electrochemical cells (Con O and Maxell) on the life-history traits of the micro-crustacean *D. magna* were demonstrated obviously. High mortality rate, delayed maturation and reproductive inhibition of the animals exposed to the leachates were recorded in the chronic exposures. However, to fully evaluate the ecological toxicity of the leachate from cells, further studies (e.g. a chemical component of batteries in detail, effects of the leachate on the other organisms, the fate of untreated batteries in the aquatic or soil environment) should be highly suggested. Besides, investigations on the effects of the leachates on life-history traits of multigenerations of *D. magna* are suggested.

5. References

Aaltonen, M., Peng, C., Wilson, B. P., & Lundstrom, M. (2017). Leaching of metals from spent lithium-ion batteries. *Recycling*, *2*, 20.

Adema, D. M. M. (1978). *Daphnia magna* as a test animal in acute and chronic toxicity tests. *Hydrobiologia*, *59*(2), 125-134.

American Public Health Association. (2012). *Standard methods for the examination of water and wastewater* (22nd ed.). Washington, DC: American Water Works Association, Water Environment Federation.

Araujo, G. S., Pavlaki, M. D., Soares, A. M. V. M., Abessa, D. M. S., & Loureiro, S. (2019). Bioaccumulation and morphological traits in a multi-generation test with two *Daphnia* species exposed to lead. *Chemosphere*, *219*, 636-644.

Barata, C., Baird, D. J., Nogueira, A. J. A., Soares, A. M. V. M., & Riva, M. C. (2006). Toxicity

of binary mixture of metals and pyrethroid insecticides to *Daphnia magna* Straus. Implications for multi-substance risks assessment. *Aquatic Toxicology*, *78*, 1-14.

Biesinger, K. E., & Christensen, G. M. (1972). Effects of various metals on survival, growth, reproduction and metabolism of *Daphnia magna*. *Journal of the Fisheries Research Board of Canada*, *29*, 1691-1700.

Chu, K. W., & Chow, K. L. (2002). Synergistic toxicity of multiple heavy metals is revealed by a biological assay using a nematode and its transgenic derivative. *Aquatic Toxicology*, *61*, 53-64.

Fisher, K., Wallén, E., Laenen, P. P., & Collins, M. (2006). *Battery Waste Management Life Cycle Assessment*. Environmental Resources Management. Retrieved from https://www.epbaeurope.net/wp-content/uploads/2016/12/090607_2006_Oct.pdf

Frías-Espericueta, M. G, Castro-Longoria, R., Barrón-Gallardo, G. J., Osuna-López, J. I., Abad-Rosales, S. M., Páez-Osuna, F., & Voltolina, D. (2008). Histological changes and survival of *Litopenaeus vannamei* juveniles with different copper concentrations. *Aquaculture*, *278*, 97-100.

Ghazy, M. M., & Habashy, M. M. (2003). Experimental toxicity of chromium to two freshwater crustaceans: *Daphnia magna* and *Macrobrachium rosenbergii*. *Egyptian Journal of Aquatic Biology and Fisheries*, *7*(3), 49-70.

Giraudo, M., Dube, M., Lepine, M., Gagnon, P., Douville, M., & Houde, M. (2017). Multigenerational effects evaluation of the flame retardant tris (2-butoxyethyl) phosphate (TBOEP) using *Daphnia magna*. *Aquatic Toxicology*, *190*, 142-149.

Jho, E. H., An, J., & Nam, K. (2011). Extended biotic ligand model for predictions of mixture toxicity of Cd and Pb using single metal toxicity data. *Environmental Toxicology and Chemistry*, *30*(7), 1697-1703.

Kim, H. Y., Lee, C. K., Lee, J. T., Moon, C. S., Ha, S. C., Kang, S. G., … Kang, M. G. (2009). Effects of manganese exposure on dopamine and prolactin production in rat. *Neuroreport*, *20*(1), 69-73.

Kooijman, S. A. L. M. (2000). *Dynamic energy and mass budgets in biological systems* (2nd ed.). Cambridge, United Kingdom: Cambridge University Press.

LeBlanc, G. A. (1982). Laboratory investigation into the development of resistance of *Daphnia magna* (Straus) to environmental pollutants. *Environmental Pollution Series A*, *27*(4), 309-322.

Luciana, R., Ulises, R., Susana, G., Horacio, T., & Maria, G. A. (2014). Effect of metals on *Daphnia magna* and cladocerans representatives of the Argentinean Fluvial Littoral. *Journal of Environmental Biology*, *35*(4), 689-697.

Meshram, P., Abhilash, Pandey, B. D., Mankhand, T. R., & Deveci, H. (2016). Acid baking of spent lithium ion batteries for selective recovery of major metals: A two-step process. *Journal of Industrial and Engineering Chemistry*, *43*, 117-126.

Muyssen, B. T. A., De Schamphelaere, K. A. C., & Janssen, C. R. (2006). Mechanisms of chronic waterborne Zn toxicity in *Daphnia magna*. *Aquatic Toxicology*, *77*(4), 393-401.

Nguyen, T. D., Vo, T. M. C, Dao, C. T., Quang, N. X., & Dao, T. S. (2016). Chronic effects of industrial wastewater on life history traits of *Daphnia magna* under the laboratory conditions. *International Journal of Agriculture and Environmental Research*, *2*(4), 1000-1012.

Okamoto, A., Yamamuro, M., & Tatarazako, N. (2015). Acute toxicity of 50 metals to *Daphnia magna*. *Journal of Applied Toxicology*, *35*(7), 824-830.

Peiro, L. T., Mendez, G. V., & Ayres, R. U. (2013). Lithium: Sources, production, uses, and recovery outlook. *The Journal of The Minerals, Metals & Materials Society*, *65*(8), 986-996.

Ramirez, D. C. S. (2014). *Tolerance of a metal adapted natural Daphnia magna population to new stressors* (Master's dissertation). Ghent University, Ghent, Belgium.

Rathore, R. S. (2001). *Studies on the use of some freshwater invertebrates as sensitive test models for the assessment of toxicity of environmental pollutants* (Doctoral dissertation). University of Lucknow, Lucknow, Uttar Pradesh, India.

Shaw, J. R., Dempsey, T. D., Chen, C. Y., Hamilton, J. W., & Folt, C. L. (2006).

Suan Sunandha Science and Technology Journal

Comparative toxicity of cadmium, zinc, and mixtures of cadmium and zinc to daphnids. *Environmental Toxicology and Chemistry*, *25*(1), 182-189.

Sterner, R. W. (2009). Role of zooplankton in aquatic ecosystems. In *Encyclopedia of inland waters* (pp. 678-688). Oxford, UK: Elsevier.

Tran, P. T., Do-Hong, L. C., & Dao, T. S. (2014). Long-term impacts of copper and chromium on survivorship, maturation, fecundity and growth of *Daphnia magna*. *Vietnamese Journal of Science and Technology*, *52*, 309-315.

Traudt, E. M., Ranville, J. F., Smith, S. A., & Meyer, J. S. (2016). A test of the additivity of acute toxicity of binary-metal mixtures of Ni with Cd, Cu, and Zn to *Daphnia magna*, using the inflection point of the concentration-response curves. *Environmental Toxicology and Chemistry*, *35*(7), 1843-1851.

U.S. Environmental Protection Agency. (2002). *Methods for measuring the acute toxicity of effluents and receiving waters to freshwater and marine organisms* (5th ed.). Washington, DC: Author.

Versieren, L., Smets, E., De Schamphelaere, K., Blust, R., & Smolders, E. (2014). Mixture toxicity of copper and zinc to barley at low level effects can be described by the Biotic Ligand Model. *Plant and Soil*, *381*, 131-142.

Wagner, M., & Oehlmann, J. (2009). Endocrine disruptors in bottled mineral water: Total estrogenic burden and migration from plastic bottles. *Environmental Science and Pollution Research*, *16*(3), 278-286.

Yasuda, K., & Tanaka, M. (2006). Report on hazardous household waste generation in Japan. *Waste Management and Research*, *24*, 397-401.

Available online at http://www.ssstj.sci.ssru.ac.th

SSSTJ

Suan Sunandha Science and Technology Journal

PM 2.5 Reduction by Installation of Façade with Broad Leaf and Narrow Leaf Plant

Akarat Panrae*, Atch Sreshthaputra

Innovation Design of Ecological Architecture Program, Faculty of Architecture, Chulalongkorn University, Bangkok 10330, Thailand

Corresponding author e-mail: ***gunthunp@gmail.com**

Received: *1 May 2020* / **Revised**: *20 May 2020* / **Accepted:** *9 June 2020*

Abstract

PM 2.5 has been an important issue for living in a city due to its negative health impact. PM 2.5 reduction by green facade was studied in this experiment. The steel facade with 3.70 x 2.50 m was installed at the front of the model room which located near the 4 lanes road. Broad leaf and narrow leaf plant as *Epipremnum aureum* and *Chlorophytum comosum* were attached to the facade for 2 weeks. The inside and outside air quality of the model room as PM 2.5, temperature, relative humidity were hourly observed. The result showed that the installation of a facade or green facade could significantly reduce PM 2.5 and heat through the model room via shading and plant evapotranspiration. Both *Epipremnum aureum* and *Chlorophytum comosum* gave better PM 2.5 reduction than steel facade which corresponding to the leaf area index (LAI) during the experiment.

Keywords: Façade, PM 2.5, Broad leaf plant, Narrow leaf plant, Green façade

1. Introduction

The worse air quality has affected people's health all over the world, causing 3.7 million deaths worldwide in 2012 due to particulate matter small than 10 µm, ozone, nitrogen oxide, and sulfur dioxide (World Health Organization [WHO], 2014). The European Environment Agency estimated that during 2012-2014, 50-63% of the Europeans would be exposed to the particle matter (PM) with a particle size of 10 µm and 85-91% to 2.5 µm. This is higher than the level informed by the World Health Organization that the concentration should not higher than 20 µg/cm^3 and 10 µg/ cm^3 for PM 10 and 2.5 µm. These small particles can cause respiratory irritation via inhalation. Moreover, some types of chemicals can be contaminated with PM 10 and 2.5 and also be passed into the body, for example, polycyclic aromatic hydrocarbon (PAH) and heavy metals (Kleeman et al., 2009). The particulate matter can also get into the circulation system triggering inflammation or blood coagulation (Seaton, Godden, MacNee, & Donaldson, 1995). The larger particulate matter originated from natural sources and human activities, while the smaller particulate matter is generated by the emission of the combustion engine (benzene and diesel) (Chow et al., 2006). Some chemical reactions are stimulated by light (Photochemical reaction) can cause even smaller dust particles and be very toxic as it can emit some heavy metals such as Polyaromatic Hydrocarbon (PAHS, Polychlorinated dibenzo-p dioxide/Dibenzofuran (PCDD/FS) Polychlorinated Biphenyl, PCB) which is a carcinogen (Dzierzanowski, Popek, Gawronska, Saebo, & Gawronski, 2011) . Planting some plants on the wall, a Green wall, could minimize the planting area, insulate a building from heat, noises and increase biodiversity in the urban area (Alexandri & Jones, 2007; Chiquet, Dover, & Mitchell, 2013; Dover, 2015; Jepson, 2016; Johnston & Newton, 2004) . A method of dust measuring has been developed by concerning factors that impact the diffusion of the dust, such as temperature, humidity, rainfall and wind speed. An ability to purify the air of each plant is different because of the different physical characteristics of each plant (shape and size) . The most ideal air-purifying plants would be the ones in the evergreen plant which do not shed their leaves in autumn (Bache, 1979; Beckett, Freer-Smith, & Taylor, 2000; Dochinger, 1980; Feer-Smith, Beckett, & Taylor, 2005; Ram et al., 2012)

This research has studied the effect of green façade installation with golden pothos (*Epipremnum aureum*) and spider plant (*Chlorophytum comosum*) were used as the broad leave and narrow leave plant for PM 2.5 passing in the building and insulation was the other advantage. Roadside room of 8 m^2 was conducted

Suan Sunandha Science and Technology Journal

and the data of dust concentration, temperature and humidity were collected.

2. Materials and Methods

2.1 Preparation the model room

The model room area 8 m^2 (2.15 x 3.70 m) was built with double layers of 12 mm thick gypsum board using a zinc structure. The door size was 0.90 x 2.0 m, the size window was 1.10 x 1.50 m and floor-ceiling was 2.50 m. This room was closed to 4 lanes road (2.00 m) and settled nearby the traffic lights.

2.2 Setting the facade

The facade was installed with steel box pipe line (25 x 25 mm), size 3.7 x 2.5 m. (length x width) and space between each pipe line was 6 x 6 cm. Installed facade was set at 0.50 m away from the room wall (Figure 1).

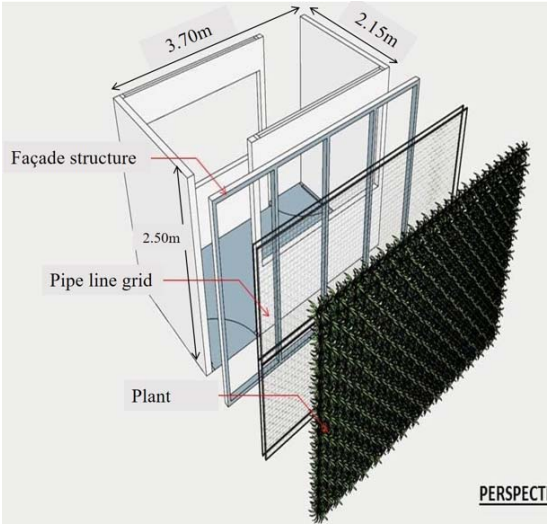

Figure 1. Show 3D model room and its dimension.

2.3 Temperature, relative humidity and PM 2.5 measurement

Thermometer/hygrometer (IBUTTON DATA LOGGER, DS-ds1921G) and particulate matter meter (SNDWAY SW-625B) were installed inside and outside the model room, 0.30 m next to the wall and 1.50 m above the room floor (inside) or pavement (outside). Hourly data were collected for each condition as 1) without façade, 2) with façade, 3) with golden pothos façade and 4) with spider plant façade. Each condition was conducted for 14 days.

2.4 Installation of green facade

The selected plants, Spider plant (*Chlorophytum comosum)* and golden pothos (*Epipremnum oureum*) were used as the representative of narrow-leaf and broadleaf plant. The Spider plant with a density leaf of 25-30 leaf/ pot and golden pothos with a density leaf of 10-15 leaf/pot were tied with the pipe line structure with 240 pots in each experiment. The planting material was a combination of soil, chopped coconut husk and monkeypod tree dry leaf, which was contained in the pot with the size of 8 x 11 x 8 cm. Water was showered on the plant pot twice a day. The experiment was conducted for 2 weeks for each condition.

2.5 Statistics data analysis

Comparability of the PM 2.5, temperature and relative humidity, in each condition in an experiment by one-way ANOVA and Least Square Difference in SPSS V. 17 program at 95% confidence level.

3. Results

3.1 Comparison of the air quality in each period

PM 2.5, temperature and relative humidity were collected hourly for 5 days (Monday-Friday) and the data were compared between outside and inside model room. These parameters were collected for 5 time periods refer to temperature grouping in Panrare, Sohsalam, and Tondee (2015). The result showed the difference of 5 time periods which are (1) 6.30-10.30 AM, (2) 10.30 AM-03.30 PM, (3) 03.30-07.30 PM, (4) 07.30 PM-00.30 AM and (5) 0.30-6.30 AM, respectively (fig 2). The car number of each period was also observed and the high amount of car period (6.30-10.30 AM, 10.30 AM-03.30 PM) resulted to a high concentration of PM 2.5 which the low temperature was the co-factor (Currie & Bass, 2008; Dzierzanowski et al., 2011). A high concentration of PM 2.5 was frequently found at low temperature and emission from car combustion was major source in urban area (Chow et al., 2006) . Low PM 2.5 was obtained at the evening (3.30-7.30 pm) due to high temperature enhances PM 2.5 dispersion to the upper atmosphere even at high car density. Low car density at night time was clearly showed low PM 2.5. The relative humidity inside the model room was high at 10.30 AM-03.30 PM because of low ventilation in the model room. According to this result, the effect of façade installation was observed during 6.30 AM-03.30 PM.

Suan Sunandha Science and Technology Journal

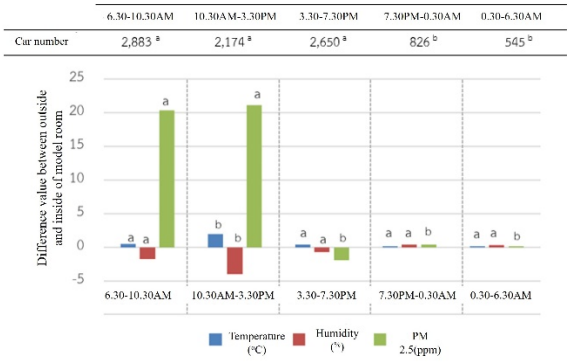

Figure 2. The differences of PM 2.5, temperature and relative humidity outside and inside model room compare with the mean number of car for 5 days (Monday-Friday) in each period.

3.2 The effect of installation façade and green facade on air quality

The PM 2. 5 concentration, temperature and relative humidity were compared during 6.30-10.30AM and 10.30 AM-03.30 PM, the difference between the outside and inside the model room (Table 1). The installation façade and green facade could reduce the amount of PM 2.5 which enters the model room significantly. The % humidity inside the model room was higher than outside due to low ventilation in the model room in 6.30-10.30 AM and resulted from plant photosynthesis in 10.30 AM-3.30 PM.

Table 1. The differences of PM 2.5 concentration, temperature and relative humidity inside and outside of the model room between 6.30-10.30 AM and 10.30 AM-03.30 PM.

Condition	6.30-10.30AM		
	Temp.	Humidity	PM2.5
No facade	0.49[a]	-1.80[a]	17.30[a]
Façade	1.24[b]	-1.22[a]	28.30[b]
Façade+Golden pothos	1.49[c]	-2.13[b]	35.63[c]
Façade+Spider plant	1.66[c]	-2.71[b]	32.40[c]
Condition	10.30AM-3.30PM		
	Temp.	Humidity	PM2.5
No facade	1.99[a]	-4.04[a]	11.09[a]
Façade	2.14[b]	-4.22[a]	14.09[a]
Façade+Golden pothos	3.09[c]	-8.00[b]	18.38[b]
Façade+Spider plant	3.66[c]	-6.11[c]	17.06[b]

Remark: The difference superscript letter in each column showed the difference between conditions at 95% confidence level.

But there may be particles matter return into the atmosphere due to wind and rain. Which the amount of heavy rain will cause the particle matter to come out of the leaves plant. (Weerakkody, Dover, Mitchell, & Reiling, 2018) The large particle matters were easily fall out of the plant leaves, while the wax which covered the plant leaf surface trapped particles matter better than smooth leaf plant. When installing the facade, the temperature inside the model room was reduced significantly ($p<0.05$) because the facade provided shade to the building. Facade with plants or green facade reduced the inside model room temperature than facades ($p<0.05$). The different plant type did not result in different temperature in both time periods. Higher difference temperature was found in 10.30 AM-3.30 PM because the high-density material outside the model room such as sidewalks and public roads accumulate heat during day time. The humidity difference between the outside and inside the building is negative. The inside of the building has humidity accumulation because ventilation is lower in the model room. Green façade installation gave a higher humidity difference ($p <0.05$). The increased humidity was caused by the photosynthesis of plants and the transpiration in the daytime and the amount of photosynthesis varied directly with the amount of solar radiation. The high difference of humidity was observed during 10.30 AM-3.30 PM because broad leaf plant (Golden pothos) gave more transpiration than narrow-leaf plants (Spider plant). This might depend on the leave areas which larger areas could give higher photosynthesis (Figure 3). While the different of plant leaves did not show the difference in PM 2.5 reduction.

a b

Figure 3. The leaf characteristics of narrow-leaf plants (a) and broad-leaf plants (b) used in the experiment.

4. Conclusion

The factors that affect the diffusion of particle matter such as temperature, humidity, rainfall, wind speed and each plant have the potential to reduce particle matter was different, especially non-deciduous plants (Bache, 1979; Beckett et al., 2000; Dochinger, 1980; Freer-Smith et al., 2005; Ram et

Suan Sunandha Science and Technology Journal

al., 2012). In the experimental area was the traffic light intersection with heavy traffic and there was high particulate matter diffusion (PM 2.5). During morning until 3.30 PM showed the highest PM 2.5 due to a large number of cars and low temperature in the morning which resulted to low dispersion of PM 2.5. But during 3.30-7.30 was the highest temperature period (Panrare et al., 2015), PM 2.5 was low because high temperature air rises up and PM 2.5 was also raised to the upper atmosphere (Beckett et al., 2000; Chow et al., 2006; Freer-Smith et al., 2005). The nearby model room could reduce PM 2.5 transfer by using a façade or green façade which could reduce PM 2.5 and temperature inside the model room. Installation of green façade, biofilter, reduced more PM 2.5 and temperature than the façade significantly ($p<0.05$). The plant could reduce wind speed, plant leave could trap particulate matter and hairy leave or wax leave could better trap particulate matter (Beckett et al., 2000; Currie & Bass, 2008; Freer-Smith et al., 2005). The broad leave (Gloden pothos) and narrow leave (Spider plant) in this study did not give the difference performance in PM 2.5 reduction. Extension of this experiment may give the difference between broad leave (Gloden pothos) and narrow leave (Spider plant) because the new plant leave will be produced and the LAI (Leave Area Index) should be further discussed.

5. Acknowledgement

This research could be discussed in both energy and plant physiology discipline by the useful advice of Dr. Prapa Sohsalam, Science and Environmental Technology Program, Kasetsart University, Kamphaeng Saen campus. The authors thank her for the great support.

6. Reference

Alexandri, E., & Jones, P. (2007). Developing a one-dimensional heat and mass transfer algorithm for describing the effect of green roofs on the built environment: Comparison with experimental results. *Building and Environment*, *42*, 2835-2849.

Bache, D. H. (1979). Particle transport within plant canopies - I. A framework for analysis. *Atmospheric Environment*, *13*(9), 1257-1262.

Beckett, K. P., Freer-Smith, P. H., & Taylor, G. (2000). Particulate pollution capture by urban trees: Effect of species and windspeed. *Global Change Biology*, *6*, 995-1003.

Chiquet, C., Dover, J. W., & Mitchell, P. (2013). Birds and the urban environment: The value of green walls. *Urban Ecosystems*, *16*, 453-462.

Chow, J. C., Watson, J. G., Mauderly, J. L., Costa, D. L., Wyzga, R. E., Vedal, S., … Dockery, D. W. (2006). Health effects of fine particulate air pollution: lines that connect. *Journal of the Air & Waste Management Association*, *56*(10), 1368-1380.

Currie, B. A., & Bass, B. (2008). Estimates of air pollution mitigation with green plants and green roofs using the UFORE model. *Urban Ecosystems*, *11*, 409-422.

Dochinger, L. S. (1980). Interception of airborne particles by tree plantings. *Journal of Environmental Quality*, *9*(2), 265-268.

Dover, J. W. (2015). *Green infrastructure: Incorporating plants and enhancing biodiversity in buildings and urban environments*. London: Routledge.

Dzierzanowski, K., Popek, R., Gawronska, H., Saebo, A., & Gawronski, S. W. (2011). Deposition of particulate matter of different size fractions on leaf surfaces and in waxes of urban forest species. *International Journal of Phytoremediation*, *13*, 1037-1046.

Freer-Smith, P. H., Beckett, K. P., & Taylor, G. (2005). Deposition velocities to *Sorbus aria, Acer campestre, Populus deltoides* x *trichocarpa* Beaupre, *Pinus nigra* and x *Cupressocyparis leylandii* for coarse, fine and ultra-fine particles in the urban environment. *Environmental Pollution*, *133*(1), 157-167.

Jepson, P. (2016). A rewilding agenda for Europe: Creating a network of experimental reserves. *Ecography*, *39*, 117-124.

Johnston, J., & Newton, J. (2004). *Building green: A guide to using plants on roofs, walls and pavements*. London: Greater London Authority.

Kleeman, M. J., Riddle, S. G., Robert, M. A., Jakober, C. A., Fine, P. M., Hays, M. D., … Hannigan, M. P. (2009). Source apportionment of fine ($PM_{1.8}$) and ultrafine ($PM_{0.1}$) airborne particulate matter during a severe winter pollution episode. *Environmental Science and Technology*, *43*(2), 272-279.

Panrare, A., Sohsalam, P., & Tondee, T. (2015). Constructed wetland for sewage treatment and thermal transfer reduction. *Energy Procedia*, *79*, 567-575.

Ram, S. S., Majumder, S., Chaudhuri, P., Chanda, S., Santra, S. C., Maiti, P. K., … Chakraborty, A. (2012). Plant canopies: Bio-monitor and trap for re-suspended dust particulates contaminated with heavy metals. *Mitigation and Adaptation Strategies for Global Change*, *19*, 499-508.

Seaton, A., Godden, D. , MacNee, W. , & Donaldson, K. (1995). Particulate air pollution and acute health effects. *The Lancet*, *345*, 176-178.

Suan Sunandha Science and Technology Journal

Weerakkody, U., Dover, J. W., Mitchell, P., & Reiling, K. (2018). Quantification of the traffic-generated particulate matter capture by plant species in a living wall and evaluation of the important leaf characteristics. *The Science of the Total Environment*, *635*, 1012-1024.

World Health Organization. (2014). *WHO's Ambient Air Pollution database: Data summary of the AAP database*. Retrieved from http://www.who.int/phe/health_topics/outdoorair/databases/cities/en/

Available online at http://www.ssstj.sci.ssru.ac.th

SSSTJ

Suan Sunandha Science and Technology Journal

Design of Plastic Medical Tray: A Case Study of Orthopaedic Implant Packaging

Nattapon Chantarapanich[1,2], Tamnuwat Valeeprakhon[2,3], Sujin Wanchat[1,3*], Melvin Stanley Veerasakul[1]

[1]Department of Mechanical Engineering, Faculty of Engineering at Sriracha, Kasetsart University, Sukhumvit Road, Sriracha, Chonburi 20230, Thailand

[2]Digital Industrial Design and Manufacturing Research Unit, Faculty of Engineering at Sriracha, Kasetsart University, Sukhumvit Road, Sriracha, Chonburi 20230, Thailand

[3]Department of Computer Engineering, Faculty of Engineering at Sriracha, Kasetsart University, Sukhumvit Road, Sriracha, Chonburi 20230, Thailand

Corresponding author e-mail: *sujin@eng.src.ku.ac.th

Received: *5 March 2020* / **Revised:** *6 May 2020* / **Accepted:** *16 June 2020*

Abstract

The plastic medical tray is commonly used for medical device packaging such as the implant or surgical instruments. The tray can be undergone gamma-ray exposure to sterilizing the medical devices inside. The tray keeps medical devices free from micro-living organisms and protects them from contaminated external environments. The plastic sheet is usually used for producing the tray which turns into a final tray shape using thermoforming. During the tray design process, factors such as the dimension of medical devices, ergonomics, and strength, have to be taken into consideration. Computer-Aided Design/Three-dimensional Printing (CAD/3DP) technologies were applied for verification of the tray geometry whereas finite element methods are applied for strength analysis. Three-dimensional (3D) models of the tray, which are referenced from the dimension of medical device, were 3D printed to test ergonomics for operating room (OR) nurses handling. After that, 3D models were evaluated the strength to ensure safety during delivery. From the analysis, the geometry of the tray was appropriate for handling with sufficient strength. The bottom corner of the tray is a critical point since it presents a high-stress magnitude. The load of 54.6 kg-f deforms the tray was less than 0.5-mm, confirming the vertical stack storage.

Keywords: Plastic medical tray, Medical device, Packaging design, Packaging analysis

1. Introduction

Medical devices, especially a long-term implanted in the body, requires sterile condition before serving to the surgery. Package for protecting medical devices away from contamination is considered as an essential requirement supplement to the implant design process. Desired characteristics of medical device packaging include sterilization compatibility, ease of forming, heat resistance during sealing, strength, and economic-scale (Bix & Fuente, 2009).

Generally, various sterilization methods are used to deactivate micro-living organisms which are autoclaves, stream, ethylene oxide gas, and gamma-ray radiation. For short-duration use invasive medical device or non-invasive medical device, the first four sterilization methods are used. However, the long term invasive implant or instrument in contact with blood such as a surgical glove, orthopaedic implant, and prosthesis, gamma-ray radiation is usually selected as a sterilization method. The gamma ray method presents the advantages in a high Sterility Assurance Level (SAL) and is simple to control. Compared to the other aforementioned techniques, they present complications in penetration in a narrow cavity, and a long period of time for the process.

Gamma-ray method uses Cobalt-60 (^{60}Co) or Caecium-137 (^{137}Ce) to generate the radiation. A-dose of 25 kGy is considered as a reference for sterilization (Silindir & Özer, 2009). In order to design the implant package which is good when undergoes gamma ray sterilization, a rigid plastic type is usually selected to make a package.

Suan Sunandha Science and Technology Journal

The shape of a package should depend on the shape of the implant. The optimal gap between package and the implant is required. The large gap may introduce the movement (momentum) of implant which could lead to damage of the package during transportation. The lower gap may be difficult to get the implant out of the package. In addition, the shape should be able to handle by operating room (OR) staff during the opening and transferring from unsterilized zone to sterilize zone.

The packages are kept in-stack to minimize the storage space in the hospital. The strength of the package is important to withstand the weight above it. Analysis of the strength can define the maximum storage package in a vertical direction. The deformation of the package could lead to a tear of plastic and eliminate the sterile conditions.

In this paper, it presents a case study of implant packaging design for humerus endoprosthesis. The endoprosthesis is intended to replace the tumor bone region, composing of four parts which are head, neck, body, and stem. The body and stem are available in three sizes in order to make it is selectable for various resection bone lengths. The requirements from the company are to design the single package which fits all parts for economic matters.

2. Materials and Methods

The design control process for the medical devices was applied to design the medical tray. The process contains six essential procedures as follows: (1) Getting user needs, (2) Identifying design input, (3) Performing design process, (4) Inspecting the design output, (5) Releasing the product, and (6) Design review. The (1) to (5) is a sequential procedure that needs to be done step-by-step. The design review in (6) is intended to be checkpoints during product development to ensure the product design is safe and effective. Thus, it has to be done in every procedure in (1) to (5). A comparison between design output in (4) and design input in (2) is “design verification”, and comparison between user needs in (1) and product performance in (5) is “design validation”. (Kinsel, 2012)

In this paper, the medical tray design process included step (1) to (5) and performed the design verification. The design validation in this case, which involves biological and clinical tests. It is beyond this scope of this paper.

The design process started by getting the user needs. The authors obtained the requirements from the medical practitioners. In addition, reviewing literature, industrial standard, product specification, drawing, and regulation relates to the design process was also performed in this step. The user needs and all related documents were summarized into design input.

In the design process, the 3D CAD models of endoprosthesis were reversely created using CAD software (VISI, Vero Software, UK). The external shape of the endoprosthesis is considered as an important shape in the design process. The unnecessary detail of the 3D model was neglected to simplify the CAD works. Endoprosthesis part has approximate bounding dimension 42 x 36 x 42 mm for head, 20 x 20 x 58 mm for neck, 18 x 18 x 76 for body, and 24 x 24 x 122 mm for stem.

After finishing the CAD design, the test for fitting was first evaluated in CAD software (VISI 21, Vero Software, UK). Then, the models of packaging and endoprosthesis were manufactured using fused deposition modeling (FDM) machine (M200, Zortrax, Poland) at Digital Industrial Design and Manufacturing Research Unit, Faculty of Engineering at Sriracha, Kasetsart University. The printed model was used to evaluate functions. Modification of the packaging model was once again revised if its functions are not met the requirements.

The following step after the 3D model was dimensionally and functionally reviewed, the 3D CAD model of packaging was evaluated the strength using the Finite Element (FE) method (ABAQUS, Dassault Systèmes, USA). In order to generate the FE model for analysis, four-node tetrahedral elements type were created based on the shape of the 3D CAD packaging model.

The evaluation was performed under various compression situations. The compression was simulated by placing the rigid plane over and under the packaging model. The upper rigid plane was controlled to displace downward. 0.5-mm, 1.0-mm, 2.0-mm, and 4.0-mm, as shown in Figure 1. Material assigned in the FE analysis was assumed to be linear elastic, in which elastic modulus and possion’s ratio has to be included. The values of material property was from tensile testing data according to ASTM D638-14 (American Society for Testing and Materials [ASTM], 2014). The

Suan Sunandha Science and Technology Journal

Equivalent Von Mises (EQV) stress of each case was compared to the yield strength of materials.

If there are no modification after reviewing the FE result, the final CAD drawing was deployed for manufacturing.

Figure 1. FE Boundary Condition**.**

3. Results and Discussion

The requirements for packaging design can be summarized as follows: (1) it has a shape which can be hold by a single hand, (2) it can be fit all components of the endoprosthesis, (3) it is feasible to manufacture with the thermoforming process, (4) it can undergo gamma ray sterilization, and (5) The package should have sufficient strength for vertical stacking.

According to the requirements, three of them were turned into design inputs which included (1) the width and length sizes of tray should be less than 180 mm (length of palm span from the tip of the thumb to the tip of the forefinger), (2) size of the tray should be covered the size of filled components, (3) the tray should be manufactured from the sheet with 0.7 mm or 1.0 mm (according to specification) and the shape must be able to release from the mold, and (4) the sheet should be in Polyethylene Terephthalate (PET) family (feasible to undergo gamma-ray sterilization).

In the design process, various engineering tools were used as tools to produce the design output as follow:

(1) For the dimension, the packaging was 150 mm length x 125 mm width x 47 mm height in dimension. With this size, the tray width was less than the size of a hand, this allows OR personal to carry on with a single hand.

(2) In addition, to dimension in (1), the tray was capable to fill components, as in Figure 2. During the development process, the 3D models of the tray and prosthesis were printed using a FDM machine to test the containing function. It was found that if the implant was filled inside, it created large movement during transportation. Therefore, the components were covered with a sterile pouch before putting into the tray to reduce the movement of the components inside the tray. The pouch pushes the cavity walls in all sides to balance the position of the components in place. In addition, the pouch also makes it is easy for OR personal to remove the pouch from the tray in sterile condition using scissor with low risk of touching the contaminated area.

(3) The tray has a taper angle of the degree to allow ejection from the mold during the thermoforming process.

(4) The edge of the tray was offset from the main portion by 8-mm, this is to stick the sterile barrier film covering on, and the choice for materials made of the tray was Polyethylene Terephthalate (PET) family. PET is suitable for making the tray and good for the radiation sterilization method (Bix & Fuente, 2009).

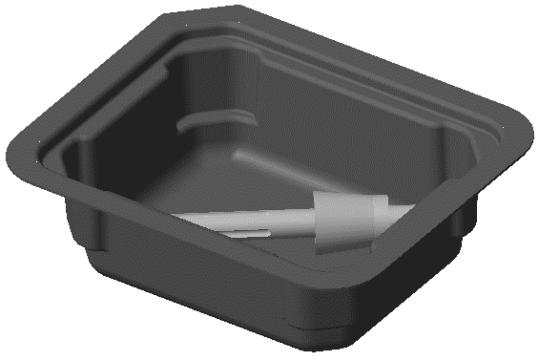

Figure 2. Tray and example of component filling test.

(5) The test for strength for vertical stacking was performed using FE analysis. The material of properties of PET (according to the selection in (4)) was tested according to ASTM D638-14 (ASTM, 2014) for gathering input for FE analysis. PET filaments were printed using a 3D printing machine (M200, Zortrax, Poland) to produce the specimen type I described in ASTM D638-14 (Tarathikhun, Chantarapanich, Valeeprakhon, & Wanchat, 2018). The specimens were used for tensile testing using Universal Testing Machine (Instron Model No. 9582, USA) at Geo-Informatics and Space Technology Development Agency (Public Organization). Three specimens were tested at a speed of 5 mm/min. The test was terminated when the specimen broke apart, as shown in Figure 3.

Suan Sunandha Science and Technology Journal

From the test, the average elastic modulus is 1,850 ± 28.5 MPa, and the average tensile strength is 39.8 ± 3.9 MPa. For possion's ratio, it was not possible to get the data from the tensile test. During the FE analysis, it was then assumed to be 0.30.

For the FE test, the thickness of PET sheet was 0.7 mm. The results showed that the high EQV stress portion of the tray was at the four bottom corners and the upper edge, as shown in Figure 3. Higher compression leads to higher stress and required more compression loads at 2.0 mm and 4.0 mm compression, the EQV stress at the upper edge is a critical level. High compression loads can cause breakage or tear at the upper edge. The stress level at 1.0 mm compression was still at risk since the high stress area is large. The safe use for tray was to allow maximum compression at 0.5 mm, which corresponds to 536.4 N (54.6 kg). This was sufficient to withstand the stack storage.

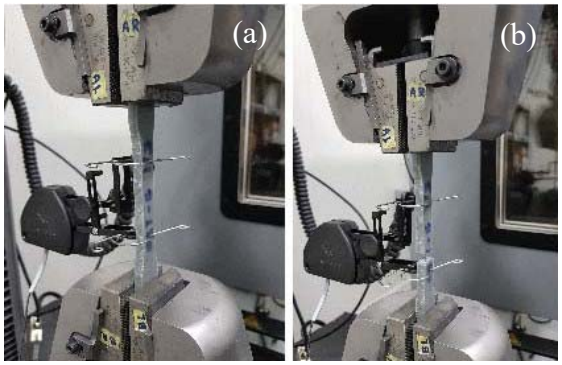

Figure 3. Material testing. (a) Test setting, and (b) Sample breakage.

As a result, the 3D model of the medical packaging tray was used for production. Figure 4 shows the finished shape of the PET tray used for the endoprosthesis.

For the design verification, design output was compared with design input. It was observed that all design output complied with the design input

There is still less work published which presents the whole design process specifically for the medical device package. Other works related to medical device package focused on cost analysis (Reymondon, Pellet, & Marcon, 2006), packaging analysis using imaging (Hindelang, Zurbach, & Roggo, 2015), and packaging materials (Wasikiewicz et al., 2008). Therefore, this current work is considered to be explained in detail paper which describing the method in medical packaging design, from design input consideration to final production.

The scope of this work focuses on the design process and its rationale in design which did not include the biological and clinical related tests of packaging i.e. bioburden, sterility test, and aging acceleration. These tests are required to determine the gamma dose used for sterilization prosthesis, the amount of microorganism exhibited on the prosthesis, and shelf life. This should be done by the manufacturer to conform ISO13485:2016 standard.

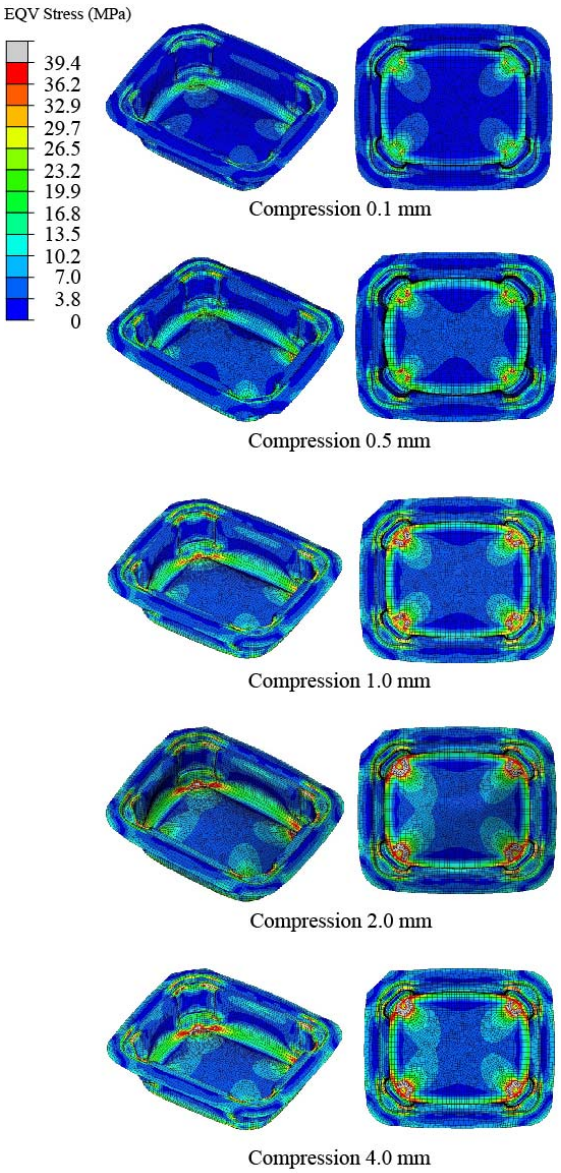

Figure 4. FE result.

4. Conclusion

This study presents the case study of

packaging design for the endoprosthesis. The characteristic required for design input includes: (1) it has a shape which can be held by a single hand, (2) it can be fit all components of the endoprosthesis, (3) it is feasible to manufacture with the thermoforming process, (4) it can undergo gamma-ray sterilization, and (5) The package should have sufficient strength for vertical stacking. The output for the design has the dimension of 150 x 125 x 47 mm with a taper shape. The materials made of the package were PET with a thickness of 0.7 mm. The package presents sufficient strength by withstanding 54.6 kg-f compression load. All design output complied with design input. In addition, the designed package has not yet included the biological and clinical related tests which should be performed in future work.

Conflict of Interest

None.

5. References

American Society for Testing and Materials. (2014). *Standard test method for tensile properties of plastics (ASTM D638-14)*. Retrieved from https://www.astm.org/Standards/D638

Bix, L., & Fuente, J. (2009). Medical device packaging. In K. L. Yam (Ed.), *The Wiley encyclopedia of packaging technology*. Hoboken, NJ: John Wiley & Sons.

Hindelang, F., Zurbach, R., & Roggo, Y. (2015). Micro Computer Tomography for medical device and pharmaceutical packaging analysis. *Journal of Pharmaceutical and Biomedical Analysis*, *108*, 38-48. doi:10.1016/j.jpba.2015.01.045

Kinsel, D. (2012). Design control requirements for medical device development. *World Journal for Pediatric and Congenital Heart Surgery*, *3*(1), 77-81. doi:10.1177/2150135111422720

Reymondon, F., Pellet, B., & Marcon, E. (2006). Methodology for designing medical devices packages based on sterilisation costs. *IFAC Proceedings Volumes*, *39*(3), 701-706. doi:10.3182/20060517-3-FR-2903.00355

Silindir, M., & Özer, A. Y. (2009). Sterilization methods and the comparison of e-beam sterilization with gamma radiation sterilization. *FABAD Journal of Pharmaceutical Sciences*, *34*, 43-53.

Tarathikhun, P., Chantarapanich, N., Valeeprakhon, T., & Wanchat, S. (2018). Mechanical properties of fused deposition modeling parts. *International Scientific Journal of Engineering and Technology*, *2*(2), 38-44.

Wasikiewicz, J. M., Roohpour, N., Paul, D., Grahn, M., Ateh, D., Rehman, I., & Vadgama, P. (2008). Polymeric barrier membranes for device packaging, diffusive control and biocompatibility. *Applied Surface Science*, *255*(2), 340-343. doi:10.1016/j.apsusc.2008.06.159